JGR Solid Earth

Key Points:

- The electrical conductivity of aqueous fluids with variable concentrations of KCl was measured to 5 GPa and 900°C
- The data show that some conductivity anomalies below cratons may be due to traces of KCl-bearing fluids
- At high pressures, KCl-bearing fluids become less conductive than fluids with NaCl, possibly due to a hydration shell collapse

Supporting Information:

Supporting Information may be found in the online version of this article.

Correspondence to:

H. Keppler,
hans.keppler@uni-bayreuth.de

Electrical Conductivity of KCl-H$_2$O Fluids in the Crust and Lithospheric Mantle

K. Vlasov[1] and H. Keppler[1]

[1]Bayerisches Geoinstitut, University of Bayreuth, Bayreuth, Germany

Abstract Evidence from diamond inclusions suggests that KCl-bearing fluids may be abundant in the subcratonic mantle and these fluids may also cause local anomalies of high electrical conductivity. We therefore measured the electrical conductivity of aqueous fluids containing 6.96, 0.74 and 0.075 wt% KCl using a hydrothermal diamond anvil cell to 2.5 GPa and 675°C, and with a piston-cylinder apparatus to 5 GPa and 900°C. We found that below 550°C, increasing pressure generally decreases solution conductivity, while at higher temperatures the effect is opposite. However, at high pressures, the conductivity of KCl in H$_2$O is smaller than for NaCl, possibly due to a hydration shell collapse. The experimental data are described by two numerical models. The first model ($R^2 = 0.999$), is preferable for crustal conditions: $\log \sigma = -2.03 + 25.0 \times T^{-1} + 0.923 \times \log c + 0.990 \times \log \rho + \log \Lambda_0$, where σ is the conductivity in S/m, T is temperature in K, c is KCl concentration in wt%, ρ is the density of pure water (in g/cm^3) at given pressure and temperature. Λ_0 is the limiting molar conductivity of KCl (in S·cm^2·mol^{-1}): $\Lambda_0 = 1{,}377 - 1{,}082 \times \rho + 6{,}883 \times 10^2 \times T^{-1} - 2{,}471 \times 10^5 \times T^{-2}$. The second model ($R^2 = 0.986$), is applicable to the lithospheric mantle: $\log \sigma = -1.52 - 357 \times T^{-1} + 0.865 \times \log c + 1.72 \times \log \rho + \log \Lambda_0$, with the same equation for Λ_0. The latter model shows that already traces of KCl-bearing aqueous fluid may account for high conductivity anomalies in the subcratonic mantle.

Plain Language Summary We measured the electrical conductivity of H$_2$O-KCl solutions of different concentrations at the conditions inside Earth's crust and mantle. We found out that such solutions have conductivities that are several orders of magnitude greater than the majority of minerals, especially in the mantle, which makes them a plausible explanation for the interpretation of deep conductive zones. Such zones are detected by geophysical remote sensing techniques and we propose that highly conductive areas in cold (<800°C) parts of Earth's mantle at a depth of 90–120 km may be due to the presence of KCl-bearing fluids. We propose equations that allow calculating the electrical conductivity of KCl-containing fluids up to 160 km depth. In addition, we observed that at the most extreme conditions of our experiments, the KCl-H$_2$O solutions have twice-smaller conductivities than NaCl-H$_2$O solutions. In contrast to this, at ambient conditions and low pressures, NaCl fluids are less conductive than KCl fluids, which implies a fundamental change in the structure of the fluid at high pressure.

1. Introduction

Potassium chloride is a common solute in various natural aqueous fluids. While the main salt component in crustal and shallow subduction zone fluids is sodium chloride (Manning, 2018; Yardley & Bodnar, 2014), multiple lines of evidence indicate that mantle fluids are often potassium-dominated (Frezzotti et al., 2012). Most of such evidence comes from the study of mantle rocks affected by metasomatism (Dawson, 2012; O'Reilly & Griffin, 2013), but there are also direct samples of high-density fluids (HDF) trapped in diamonds (e.g., Izraeli et al., 2001; Rege et al., 2010). While fluids released by dehydration of subducted slabs will be rich in NaCl, upon percolation through the mantle, the K/Na ratio will increase as K is much more incompatible than Na in normal mantle minerals (Izraeli et al., 2001). This is likely the origin of KCl-rich fluids in the upper mantle.

With salt concentrations typically at the levels of brines (Frezzotti & Ferrando, 2018; Frezzotti & Touret, 2014; Frezzotti et al., 2012), saline solutions are highly conductive at mantle conditions, as already demonstrated for NaCl-bearing fluids (H. Guo & Keppler, 2019). Zones of elevated conductivity possibly associated with saline fluids are detected via magnetotelluric surveys above subducting plates (Evans et al., 2014; Pommier & Evans, 2017) or in areas of ongoing lithospheric mantle metasomatism (Patkó et al., 2021). However, a very intriguing case of possible fluid presence in the lithospheric mantle comes from the Slave (Canada) and Kaapvaal
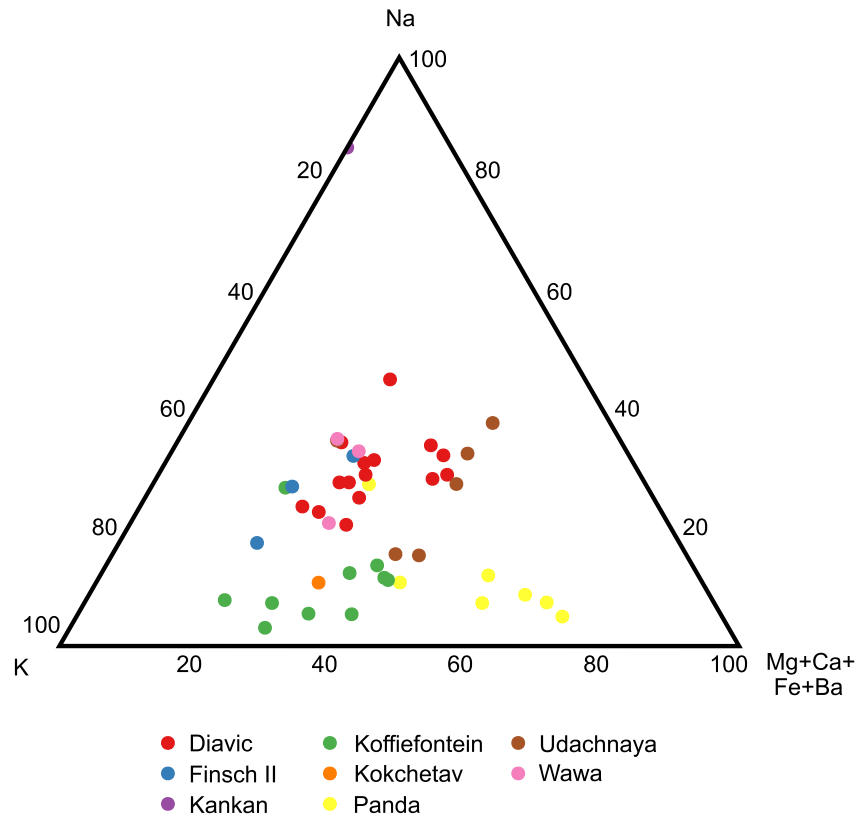
Figure 1. Average and individual compositions of brine inclusions (in mol%) in diamonds from Diavic (Klein-BenDavid et al., 2004, 2007), Finsch II (Weiss & Goldstein, 2018; Weiss et al., 2014), Kankan (Weiss et al., 2014), Koffiefontein (Izraeli et al., 2001), Kokchetav (S. L. Hwang et al., 2005), Panda (Tomlinson et al., 2006), Udachnaya (Zedgenizov et al., 2007) and Wawa (Smith et al., 2012). Si: 0–7.9 mol%, Avg. 4.1 mol%; Cl: 21.9–52.1 mol%, avg. 37.7 mol%.

(South Africa) cratons, were kimberlites, known to produce diamonds with potassic HDF's, coexist with conductive anomalies at estimated diamond formation depths.

In the interior of the Slave craton, a highly conductive zone, known as the Central Slave Mantle Conductor (CSMC; Jones et al., 2001, 2003), with resistivity of 10–15 $\Omega \cdot$m originates at 80–120 km and descends to ~200 km. The Eocene kimberlite field is located above this conductor with the Diavic (Klein-BenDavid et al., 2004, 2007) and Panda (Burgess et al., 2009; Tomlinson & Müller, 2009; Tomlinson et al., 2006) kimberlites providing samples of potassium-rich fluids from ~150 to 200 km. Similarly, in the lithospheric mantle of the Kaapvaal craton, multiple mantle conductors (Evans et al., 2011) may be explained by the presence of fluids. Mineralogical evidence suggests the migration of potassic fluids (Konzett et al., 2013), in agreement with inclusions from diamonds of the Koffiefontein (Izraeli et al., 2001, 2004) and Finsch Group II kimberlites (Weiss & Goldstein, 2018; Weiss et al., 2014), see Figure 1. The conductors at 80–200 km depth below the Dharwar craton (Kusham et al., 2018, 2019, 2021) are another possible case with diamondiferous kimberlites present at the craton, but no "direct sampling" of fluids reported so far. On the other hand, there are samples of potassic fluids from kimberlite diamonds of Jwaneng in Botswana (Schrauder & Navon, 1994; Schrauder et al., 1996) and Udachnaya in Russia (Zedgenizov et al., 2007), but those areas are not yet covered by large-scale magnetotelluric surveys.

KCl-rich fluid inclusions have been reported not only from kimberlitic diamonds, but from metamorphic ones as well. Such samples were discovered in ultra-high-pressure (UHP) rocks of the Kokchetav UHP complex, where diamonds with potassium-rich HDF's (Dobrzhinetskaya et al., 2005; S. L. Hwang et al., 2005) occur together with ample evidence of fluid and melt-related metasomatism (Mikhno et al., 2014; Schertl & Sobolev, 2013). High-pressure potassic hydrous phases, such as as K-cymrite (Mikhno et al., 2014; R. Y. Zhang et al., 2009) or maruyamaite (Lussier et al., 2016) found in the Kokchetav rocks may transport both water and potassium deep

into the mantle. Though this particular terrain may not be representative for UHP metamorphism in general, it provides a valuable example of a possible scenario that may apply even to current zones of continental crust subduction (e.g., Seno & Rehman, 2011).

Numerical interpretation of magnetotelluric data, for example, a direct estimate of the amount of possible fluid or melt in the mantle and its concentration, requires electrical conductivity data measured at mantle conditions (Pommier, 2014). Yet for potassium chloride-rich aqueous fluids such measurements have not been reported.

Being a standard solution for electrochemical cell calibration, KCl aqueous solutions are well studied at low pressures and temperatures, with an extensive compilation of more than a hundred years of measurements provided by Corti (2008). Unfortunately, the majority of the data from this summary was collected for very dilute solutions (<0.01 m or <0.075 wt%), as part of limiting molar conductance studies, and is not very useful for geological purposes. Electrical conductivity values for solutions with KCl content in the range of naturally occurring fluids were reported by J. U. Hwang et al. (1970) (0.12–3.96 m, 0.89–22.8 wt%) and Sharygin et al. (2002) (0.001–4.5 m, 0.0075–25.12 wt%), but the maximum P-T conditions achieved by both studies are 600°C and 300 MPa. Mangold and Franck (1969) managed to successfully measure 0.01 m KCl solution to 1000°C and 1,386 MPa. However due to technological limitations, more extreme conditions remained experimentally inaccessible until recently. Based on newly developed high-pressure high-temperature electrochemical techniques, this study presents electrical conductivity measurements of 0.075–6.96 wt% solutions to 900°C and 5 GPa, covering a wide range of possible lithospheric mantle conditions and fluid concentrations.

2. Experimental Methods

2.1. Overview of the Experimental Strategy

The general experimental procedure is similar to the one adopted by H. Guo and Keppler (2019) in their study of the conductivity of aqueous NaCl solutions. First, the conductivity of KCl solutions was measured in a restricted range of pressures and temperatures (up to 2.5 GPa and 675°C) using externally heated diamond anvil cells (DAC) with two metal gaskets as electrodes, separated by a perforated diamond platelet. Based on these data, a first numerical model of fluid conductivity as a function of density, temperature, concentration and limiting molar conductivity was calibrated. Second, data were acquired with a piston-cylinder (PC) electrochemical assembly up to 5 GPa and 900°C. In these experiments, the conductivity of an aggregate of diamond powder with the KCl solution in the pore space was measured. In order to extract the pure fluid conductivity, the effective fluid fraction in this aggregate has to be calibrated. This could be done at ambient conditions after the run or under pressure in the low-temperature region, where conductivity changes only slightly with pressure. The latter approach was applied here, by modest extrapolation of the electrical conductivity model from the DAC experiments. H. Guo and Keppler (2019, their Figure 4b) demonstrated that this approach yields results that are in excellent agreement with a calibration after the run at ambient condition.

The procedure used in this study results from the technological limitations of the two experimental setups. The DAC electrochemical cell allows to access a limited pressure-temperature range but yields data with good precision. The PC cell may cover a wider range of pressures and temperatures, but requires external conductivity values for low temperature calibration.

2.2. Diamond Anvil Cell Electrochemical Assembly

Fluid conductivities up to 2.5 GPa and 675°C were measured in the DAC using an assembly similar to that developed by Ni et al. (2014), see Figure 2a. A Bassett type externally heated diamond anvil cell (Bassett et al., 1993) with 0.7 mm culet type I diamonds and two iridium gaskets, separated by a diamond platelet, was loaded with the fluid of choice and measured. The cell was heated by two molybdenum coils around the tungsten carbide diamond seats. Temperature was measured with a precision of ± 5°C by two type K thermocouples in contact with the upper and lower diamonds. During the experiment, the cell was flushed with an Ar-H$_2$ (2%) mixture to prevent heater oxidation.

Two types of insulating diamond platelets were used: (a) single crystal synthetic CVD diamond (0.3 mm thickness, 0.7 mm diameter, 50-μm pinhole) and (b) polycrystalline "HIME-DIA" diamond (Irifune et al., 2003; 0.5 mm thickness, 1.5 mm diameter, 100-μm pinhole). We achieved maximal pressures of 2.5 GPa with the
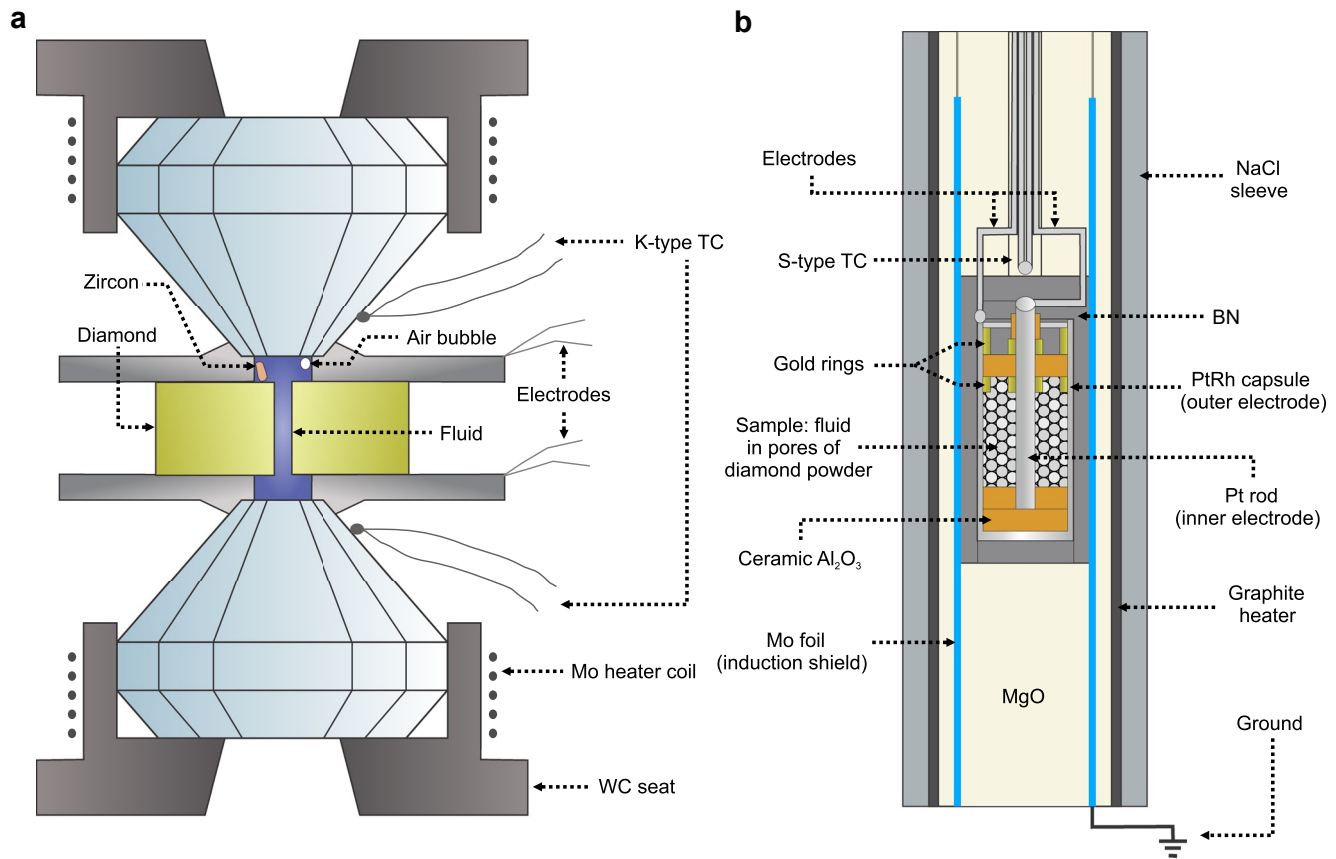
Figure 2. Devices used for electrical conductivity measurements at high pressure. (a) Externally heated diamond cell with two electrodes separated by perforated diamond platelet. (b) Piston-cylinder electrochemical cell, based on a standard ½'' assembly. Note the gold rings introduced to improve sealing.

single crystal diamonds without failure. Iridium gaskets were 250 μm thick, doubly polished, with a hole ranging from 300 to 150 μm, depending on the target pressure of the experiment. Before the run, drilled gaskets were pre-indented using a solid diamond disc to significantly reduce cell deformation.

Natural zircon crystals (Sri Lanka, annealed at 900°C for 20 hr) placed in the upper cell chamber were used as pressure sensors (Schmidt et al., 2013), with pressure being calculated based on the shift of the 1008.1 cm^{-1} Raman band. The cell was loaded with 1, 0.1 or 0.01 M KCl conductivity standards (Fluka Analytical, 1 M stands for a concentration of 1 mol/l at standard conditions), equivalent to 6.96, 0.74 and 0.075 wt% KCl concentrations used later throughout the article. The gaskets served as electrodes and were connected by two wires each to the Solartron-1260 impedance analyzer after closuring the cell. Finally, fluid density was adjusted by varying the size of the bubble in the cell.

Raman spectra necessary for pressure calculation were collected with a Horiba Labram 800 HR UV confocal Raman spectrometer using the 514 nm line of an argon laser at 100 mW output power, a 1,800 mm^{-1} grating and a confocal pinhole of 100 μm. In some experiments, where the location of the pressure sensor did not allow to measure the band shift due to diamond platelet luminescence, fluid density was determined based on the homogenization temperature (vapor bubble disappearance). Usually the difference between homogenization and nucleation (vapor bubble reappearance on cooling) temperatures was 5°C or less, which implies isochoric behavior and allows to calculate pressures based on the equation of state of pure water (Wagner & Pruß, 2002).

For converting measured bulk resistances R to fluid conductivity σ, some calibration of the cell constant is required:

$$K_{cell} = \sigma_{fluid} * R_{bulk} \qquad (1)$$

Closed cells were calibrated at ambient conditions using the known conductivities of KCl solutions at room temperature (Wu et al., 1991). Mostly, K_{cell} depends on the geometry of the pinhole in the diamond platelet, with a lesser contribution from the distances between the hole and the electrodes. The latter, as noted previously by Sinmyo and Keppler (2017), is affected by the cell deformation. However, the use of pre-indentation, due to the rigidity of iridium, allowed to almost completely eliminate that effect with the cell constants measured before and after experiment differing by less than 5%. A comparable factor that contributes to the K_{cell} determination error is the limited precision of temperature measurements during the calibration process itself, due to the precision of the K-type thermocouples and their placement. The conductivity of the 0.075 wt% KCl at 20°C and at 25°C differs by 10% and a possible error introduced by just moving the experimental assembly from one room to another probably exceeds the K_{cell} value drift due to changes in geometry.

2.3. Piston-Cylinder Electrochemical Assembly

Unfortunately, the mechanical properties of the diamond platelets and iridium gaskets limit the pressure-temperature range accessible with the DAC setup. To expand it to 5 GPa and 900°C, we used a separate PC apparatus assembly, based on the standard ½'' NaCl-MgO PC cell design and the same KCl standard solutions. Originally developed to explore the electrical conductivity of melts by Ni, Keppler, Manthilake, and Katsura (2011) it was modified and adapted for fluids by H. Guo and Keppler (2019).

The $Pt_{95}Rh_5$ capsule and a central Pt rod serve as electrodes and a layer of diamond powder (40–60 μm grain size, Alfa-Aesar), filled with a fluid, is located between them (Figure 2b). The rod is held in place by ceramic alumina discs, with the top one also serving as a sealing cap for a diamond trap. A layer of pyrophyllite below the capsule cap seals the setup and the cap is insulated from the rod by a ceramic alumina sleeve. For this study, gold rings above and below the top ceramic alumina ring were added, to provide better sealing between the ring and the capsule wall. A friction correction of 5% was applied to the nominal pressure, according to calibration of the quartz-coesite transition at 790°C (Bose & Ganguly, 1995). The cell is protected from the inductive effect of the heater by a Faraday cage, made out of 0.125 mm thick molybdenum foil. An S-type ($Pt-Pt_{90}Rh_{10}$) thermocouple was used for temperature measurements.

Fluid conductivity can be extracted from the measured bulk cell resistances. This may be demonstrated by an application of the Hashin-Shtrikman upper bound (HS⁺) model (Hashin & Shtrikman, 1962) that describes the bulk conductivity of a fluid-solid aggregate as a function of the individual phase conductivities and the fluid fraction, with the assumption that the fluid forms an interconnected network:

$$\sigma_b = \sigma_f + \frac{3(1 - \varnothing)\sigma_f (\sigma_d - \sigma_f)}{3\sigma_f + \varnothing (\sigma_d - \sigma_f)} \tag{2}$$

where σ_b is the bulk conductivity of the aggregate, $\varnothing$ the fluid fraction, σ_f is the fluid conductivity and σ_d is the conductivity of diamond. Previous studies (Vandersande & Zoltan, 1991) demonstrate that the electrical conductivity of diamond within our experimental range is very low, ranging from 10^{-14} S/m at 25°C to 10^{-4} S/m at 900°C, and thus can be neglected relative to σ_f without introducing significant errors. This yields

$$\sigma_b = \sigma_f \left(1 - \frac{3(1 - \varnothing)}{3 - \varnothing} \right) \tag{3}$$

Equation 3 demonstrates that fluid conductivity can be calculated based on the measured bulk conductivity of the cell if the fluid fraction and cell physical dimensions are known. While the cell geometrical parameters can be measured directly, the fluid fraction estimation is complicated. A way to estimate it was proposed by H. Guo and Keppler (2019), based on HS⁺ model applied to the post-run measurements of the assembly at ambient conditions, or alternatively, by a calibration under pressure at low temperatures, where the pressure effect on fluid conductivities is small.

Therefore, our bulk measurements were evaluated based on the extrapolation of the KCl conductivity model obtained through DAC measurements. As Equation 3 remains valid at any temperature and pressure, the cell constant can be evaluated at any experimental conditions if fluid conductivity is known. Though our electrical conductivity model was established on the data up to 2.5 GPa and 675°C, the model itself suggests that at 400°C
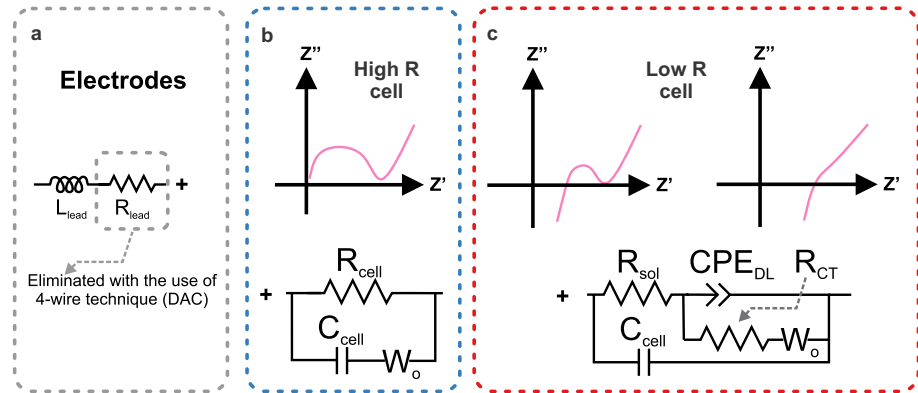
Figure 3. General equivalent circuit, modeling the impedance responses of electrochemical setups used in this study: (a) simplified circuit representing the response of the electrodes; (b) cell of high resistance (R, Ω) for example, response of the cell containing KCl solutions of low concentration or a mixture of saline ice and diamond powder; (c) cell of low resistance (R, Ω) for example, response of the cell containing KCl-rich fluid in the pores of diamond powder. Each given cell is a combination of (a and b) or (a and c), depending on the conditions.

the pressure influence on conductivity is quite minor and the extrapolation would not contribute significantly to the overall error of the measurement. Thus:

$$K_{\text{cell}} = \sigma_{400} * R_{400} \tag{4}$$

where σ_{400} is calculated based on Equation 5 (see below) and R_{400} is measured directly.

2.4. Impedance Data Acquisition and Treatment

For both experimental devices, impedance was measured from 1 MHz to 2 kHz or less using a Solartron-1260 impedance analyzer, with a voltage amplitude of 700 mV. The accuracy in resistance measurements with this instrument is specified by the manufacturer as 0.1% for the range of 10 Ω–100 kΩ at 10 kHz.

Despite major constructive differences, the impedance response of both the PC and the DAC electrochemical cells is governed by the same physicochemical principles. Each of them features two noble metal electrodes separated by comparable distances (1.7 and ~1 mm respectively) and the same type of fluid. Diamond powder, present in the PC assembly, does not contribute to the measured conductivity according to Equation 3, providing only a non-reactive framework. This statement is supported by tests at ambient conditions that demonstrated the same type of impedance response in a PC assembly filled with fluid without diamond powder ($\emptyset = 1$) and with diamond powder containing variable fluid fractions.

The full impedance response of a system consisting of two noble metal electrodes and a binary aqueous electrolyte is traditionally described by an equivalent model circuit known as a Randles cell (Barsoukov & Macdonald, 2005; Lvovich, 2015; Randles, 1947). Figure 3 shows a slightly modified version of it, which we adopted to interpret the observed impedance responses from our assemblies (Figure 4).

L_{lead} and R_{lead} (Figure 3a) describe the contribution of the lead wires to the measured impedance. Both of those values depend on the physical parameters of the electrodes, connecting the cell and the measuring device. The DAC setup utilizes four-wire measurements and therefore allows to avoid the R_{lead} contribution, with lead length of only ~7 cm, which significantly lowers L_{lead}. In theory, the 4-wire setup also allows to avoid the lead inductive contribution. However, this is rarely achieved in real high pressure-high temperature experiments due to the length and placement and imperfect connections of the wires (Savova-Stoynov & Stoynov, 1987). Measurements of the PC electrochemical cells were performed with a two-wire technique (lead length of ~60–25 cm) and required correction for lead resistances, that were collected before the runs using a short-circuit procedure (Ni, Keppler, & Behrens, 2011).

A response from the electrochemical cell itself (Figures 3b and 3c) consists of the following parts: R_{sol} is solution resistance, C_{cell} is the geometric capacitance of the cell, CPE_{DL} is a capacitance of the electrochemical
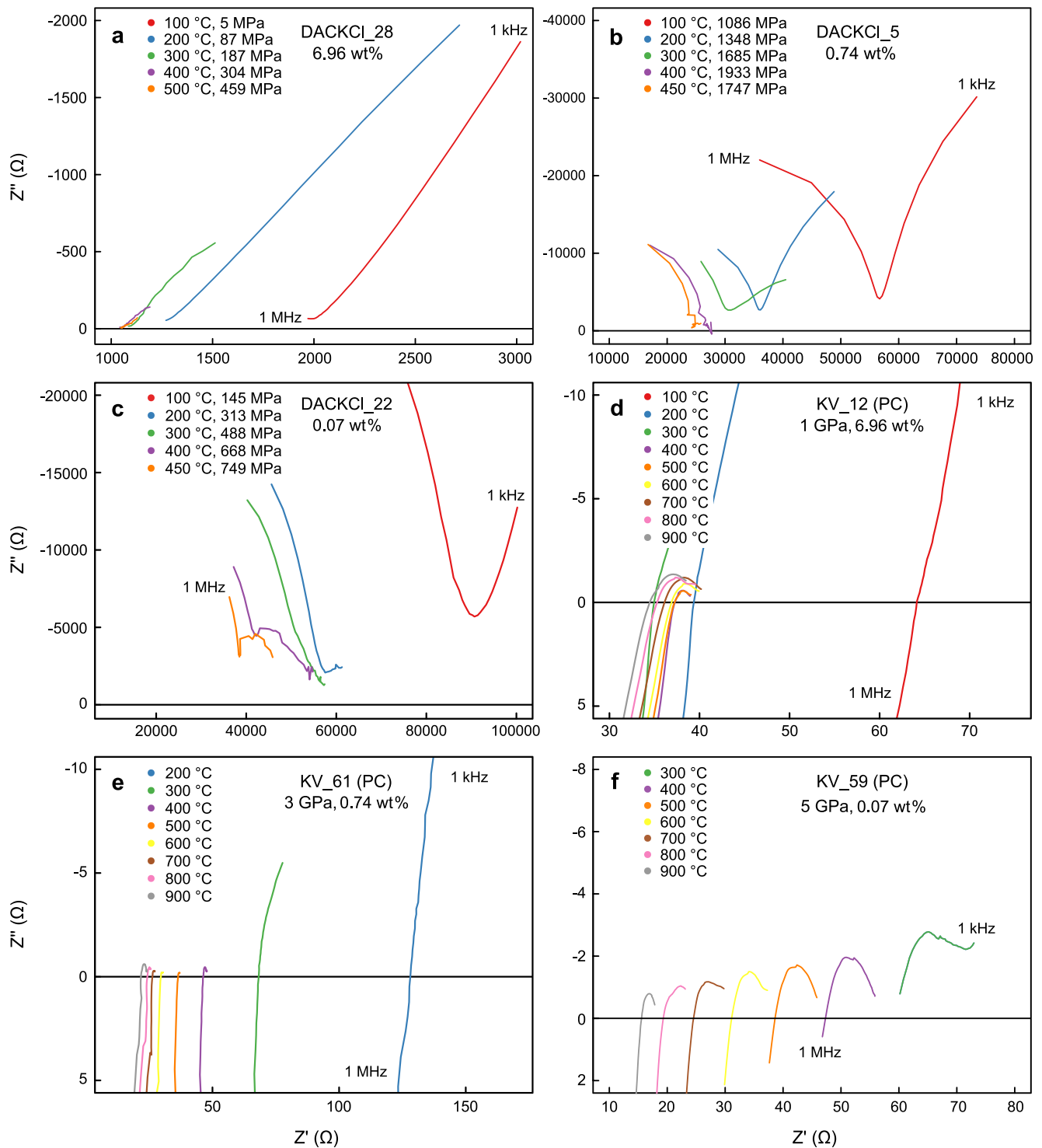
Figure 4. Nyquist plots for impedances measured in: (a–c) diamond anvil cell assemblies, (d–f) piston-cylinder assemblies. Analog circuits and fitting results for selected measurements presented here are available in Figures S1–S7 of Supporting Information S1 and Table S5 of Supporting Information S2.

double layer modeled with a constant phase element, R_{CT} is charge transfer resistance and W_o is an open Warburg element. C_{cell} in case of both assembly types is governed by the placement and area of the opposing electrodes as well as dielectric properties of all materials contained between them. The CPE_{DL} and R_{CT} contributions are not resolved on impedance diagrams if $R_{sol} \gg R_{CT}$ and a small semi-arc corresponding to electrode polarization
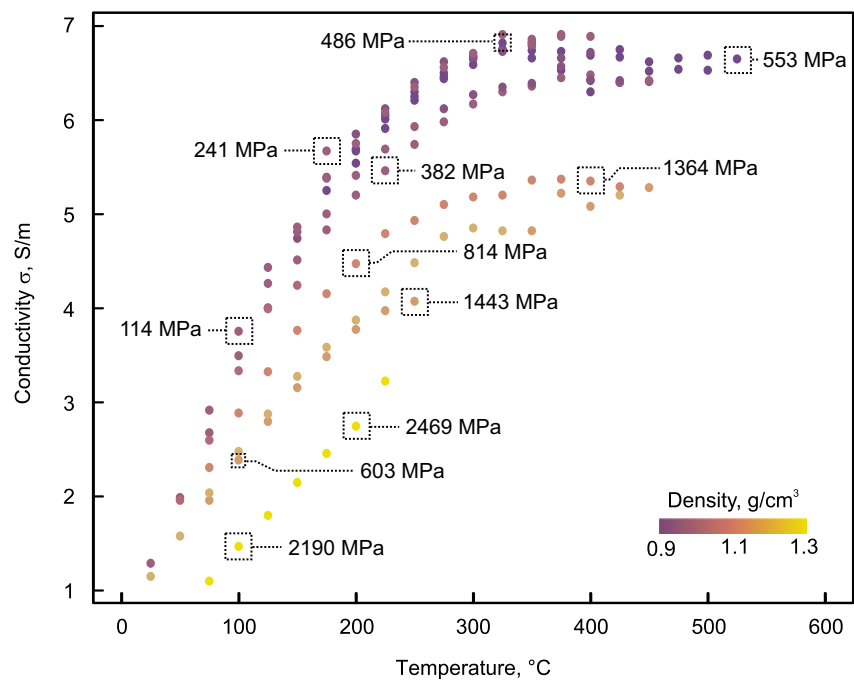
Figure 5. Electrical conductivities of the 0.74 wt% KCl as functions of density and temperature.

appears on Nyquist plots only at elevated temperatures as fluid resistance decreases. Thus, for cells with high sample resistance those elements can be omitted (Figure 3b). The Warburg impedance, attributed to charge diffusion in the electrolyte or ice, is present in all acquired data, however it is not always perfectly and completely resolved in high temperature data as it occupies the region of low frequencies (<1 kHz–100 Hz) that is prone to various interference such as noise from the heating circuit. The main purpose of this model is to describe the features observed in impedance measurements performed in the field of liquid water stability. Below freezing temperature, the right part of the circuit, corresponding to the cell impedance response, turns into a true parallel arrangement of the resistor and capacitor (Figure 3b), as expected for a polycrystalline solid. This phase transition is an important part of the measurement procedure at high pressures, however we do not report any saline ice conductivity values as it is beyond the scope of the present paper.

Not all elements of the aforementioned model can be precisely extracted from our impedance data, as the cell designs and experimental conditions vary significantly. However, the solution resistance (R_{sol}), which is the only variable relevant for this study, can always be reliably obtained with the accuracy of <0.1 Ω. To achieve this, we fitted measured impedances using simplified versions of our analog circuit model, which feature main elements observed in each particular case. For example, C_{cell} was commonly omitted from the simplified models due to induction, and the low-frequency Warburg element was modeled as a parallel arrangement of CPE and R with arbitrary large resistance. Typical examples for the different kinds of fits used for both diamond anvil cell and PC impedance spectra are given in Figures S1–S7 of Supporting Information S1 with fitting parameters available in Table S5 of Supporting Information S2.

3. Results

3.1. Conductivity Measurements in the DAC Assembly

Data collected across all three concentrations of potassium chloride in the DAC-based electrochemical assembly was compiled into a data set (Table S1 in Supporting Information S2). Densities were calculated based on the known pressures from the equation of state by Wagner and Pruß (2002).

Part of that data set, representing the conductivities of 0.74 wt% KCl fluid, can be seen in Figure 5. In general, increasing KCl concentration increases conductivity. Values measured for 0.075 and 0.74 wt% solutions differ

approximately tenfold, with the ratio between 0.74 and 6.96 wt% values being slightly smaller. This can be attributed to a decrease in the degree of KCl dissociation with the increase of the concentration itself.

For all concentrations, within the temperature-density range of our experiments, we observe two effects that have an opposing influence on conductivity: σ increases with the increase of temperature and decreases with the increase in density. The temperature effect can be explained with the increase in ion mobility at elevated temperatures (Marshall & Frantz, 1987; Quist & Marshall, 1968).

At fixed temperature, the increase in pressure and therefore in density leads to two opposing physical effects. First, increasing density increases the dielectric constant, which is a factor promoting dissociation of KCl into K^+ and Cl^-. Higher dissociation means that more charge carriers are available in the solution and the conductivity rises. This effect is obvious at low temperatures and low densities. For example, at 300°C, an increase in fluid density up to 0.9 g/cm³ leads to a gradual increase in conductivity. However, increasing fluid density impedes ion mobility and above 0.9 g/cm³ this effect reduces conductivity (Mangold & Franck, 1969). This data set was used to produce a numerical model, describing the electrical conductivity of the KCl aqueous fluid in crustal conditions as a function of density, concentration, temperature, and limiting molar conductivity.

3.2. Conductivity Model for KCl-Bearing Aqueous Fluids in the Crust

We used the diamond anvil cell data to calibrate a model for predicting electrical conductivities of KCl-H₂O fluids in the crust. This model will also be used for the low temperature calibration of PC fluid conductivity measurements. As shown by Sinmyo and Keppler (2017) in their study of NaCl-bearing fluid, the following model yields a very good agreement with experimental measurements:

$$\log \sigma = A + B * T^{-1} + C * \log c + D * \log \rho + \log \Lambda_0 \tag{5}$$

where σ is the conductivity of the fluid, T is the temperature in Kelvin, c is the concentration in weight percent, ρ is the density of pure water at given P and T in g/cm³, Λ_0 is a limiting molar conductivity at infinite dilution in S·cm²·mol⁻¹. Coefficients A, B, C, D are determined by least squares regression of the DAC experimental data set. While temperature, concentration and density are known parameters for any particular composition and conditions, Λ_0 at those conditions needs to be calculated separately. Mangold and Franck (1969) demonstrate in their study of the limiting molar conductivity of KCl aqueous fluid that with increasing density, the value of Λ_0 decreases linearly within the range studied (from 0.7 to 1.2 g/cm³). Increasing temperature increases Λ_0 up to 400°C, but has very little effect above 400°C. Thus, the limiting molar conductivity can be described by the following empirical model:

$$\Lambda_o = \lambda_1 + \lambda_2 * \rho + \lambda_3 * T^{-1} + \lambda_4 * T^{-2} \tag{6}$$

with coefficients $\lambda_1 - \lambda_4$ being determined by a multiple regression fit of Λ_0 values provided by more contemporary measurements of Ho and Palmer (1997) and Sharygin et al. (2002). Performed in smaller range of densities and temperatures they appear to be more precise than the limiting molar conductivities provided by Mangold and Franck (1969) and Ritzert and Franck (1968). This choice of calibration data results in a better approximation of the high density and low temperature region.

The numerical fit obtained ($R^2 = 0.956$) yielded $\lambda_1 = 1{,}377 \pm 187$, $\lambda_2 = -1{,}082 \pm 69$, $\lambda_3 = 6{,}883 \times 10^2 \pm 2{,}383 \times 10^2$, $\lambda_4 = -2{,}471 \times 10^5 \pm 752 \times 10^5$. Being mostly empirical, this equation provides best performance on data within its calibration range. This range fully encompasses the conditions of our DAC measurements and even most of the PC measurements. With Λ_0 given by Equation 6, a regression fit was carried out for Equation 5. To achieve best fit quality, the full set of our 6.96, 0.74 and 0.075 wt% KCl fluid electrical conductivity values (353 data points, Table S1 in Supporting Information S2) was merged with the data for 0.075 wt% solution by Mangold and Franck (1969) (60 data points), to compensate for the decrease in precision of the method used at low concentrations. Since there is no data for Λ_0 available below 200°C, we excluded values below 175°C from the resulting data set (323 data points total) to avoid the influence of the increasing uncertainties of Equation 6 on our fit.

The fitting procedure ($R^2 = 0.999$) resulted in $A = -2.03 \pm 0.01$, $B = 25.0 \pm 5.39$, $C = 0.923 \pm 0.002$, $D = 0.990 \pm 0.037$. As seen from Figure 6a, these fit parameters provide valid conductivity predictions for all values within the specified range of DAC measurements.
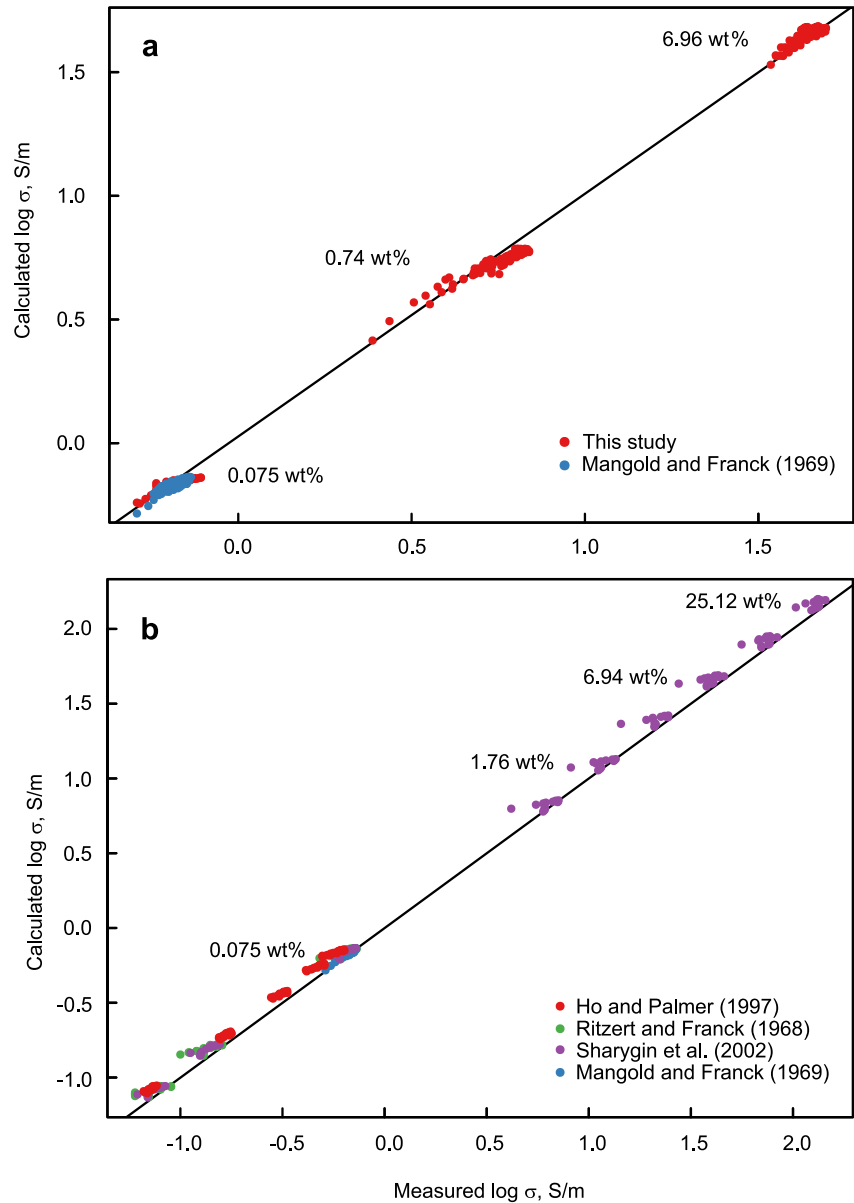
Figure 6. Numerical model for KCl-H_2O fluid conductivity data from diamond anvil cell measurements. (a) Comparison of measured fluid conductivities and values predicted by Equation 5. (b) Test of Equation 5 against existing fluid conductivity data ($\rho \geq 0.6$ g/cm^3). Measurements of Mangold and Franck (1969) (blue) used for the creation of the model are given as a reference.

To test the performance of the model we compared its predictions with KCl fluid conductivity measurements from three other studies (Ho & Palmer, 1997; Ritzert & Franck, 1968; Sharygin et al., 2002), see Figure 6b. For KCl concentrations up to 25.12 wt%, predictions appear to be quite accurate (347 data points, $R^2 = 0.999$) for measurements within the ρ-T-c range of our numerical model. Predictions strongly deviate from the measurements for $\rho < 0.6$ g/cm^3, but this is expected as these densities are far beyond our calibration data. For predicting conductivities in the shallow Earth's crust at such low densities, Equation 5 should therefore be used with caution.

3.3. Conductivity Measurements in the Piston-Cylinder Assembly

With Equation 5 established, the K_{cell} for the PC electrochemical cell was calculated, based on the fluid conductivity estimate at 400°C. This calibration introduces only limited uncertainties, as the conductivity shows only a
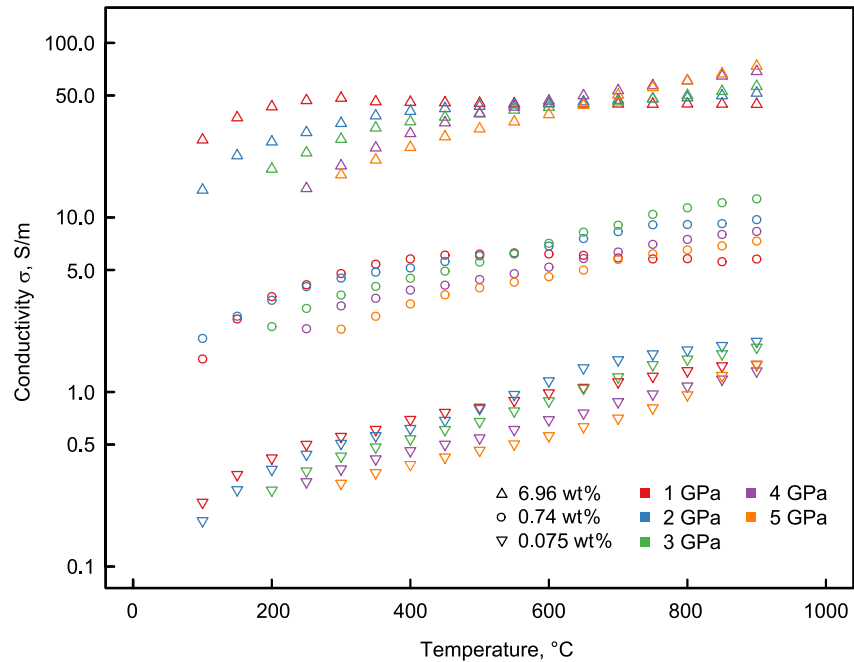
Figure 7. Electrical conductivities of the 6.96, 0.74, and 0.075 wt% aqueous solutions measured in a piston-cylinder electrochemical assembly.

minor dependence on fluid density at 400°C. Fluid conductivities in the whole measurement range from 100 to 900°C and from 1 to 5 GPa were then calculated, assuming that the cell constant remained essentially the same at all temperatures. Measured cell resistances and compilation of resulting conductivity data are available in Tables S2 and S3 of Supporting Information S2 respectively. Figure 7 shows measured conductivities at some pressures as function of temperature.

As seen from Figure 7, the influence of pressure and temperature on the electrical conductivity of the H_2O-KCl fluids is the same as for data collected with the diamond anvil cell electrochemical assembly. With increasing density, fluid conductivity decreases below 550°C due to the decrease in ion mobility. At 3, 4, and 5 GPa and below 200, 250, and 300°C respectively, conductivities tend to differ very little for each concentration as the samples were mostly a mixture of ice and diamonds at those conditions (Journaux et al., 2013) and such measurements were omitted from the data set. Above 550°C, for each pressure an increase in temperature generally increases conductivity. However, the maximum measured conductivity and the pressure at which this value is recorded appears to be dependent on the KCl concentration.

At higher pressures, the effect of the increased density on ion mobility seems to overpower the effect of the changing dielectric constant. While for 6.96 wt% KCl measured conductivities at 900°C increase with pressure, for 0.74 and 0.075 wt% this is true only to 3 and 2 GPa respectively. At higher pressures and for 0.74 and 0.075 wt% fluids, the value of conductivity tends to decrease. This effect was also previously observed in NaCl-containing fluids by H. Guo and Keppler (2019).

For 6.96 and 0.74 wt% concentrations, the measured values at 1 GPa are in agreement with the DAC equation predictions. However, the corresponding values for 0.075 wt% KCl solution at temperatures above 500°C tend to be ~20% higher than those measured by Mangold and Franck (1969). Due to the extremely low values of conductivities measured, it is difficult to provide a definitive explanation for this effect, as the data may be very sensitive to minor contaminations of the fluid and other effects.

To better constrain the KCl fluid conductivity, multiple experiments were carried out for each pressure of 6.96 and 0.74 wt% concentrations (see Tables S2 and S3 in Supporting Information S2). As illustrated by Figure S8 in Supporting Information S1, for both concentrations the method produces very similar data. For pressures of 3 GPa and above, the leakage of the assembly becomes a significant source of error. In general, each new cooling cycle in this method produces slightly higher resistances at high pressure and low temperatures due to fluid leaks,
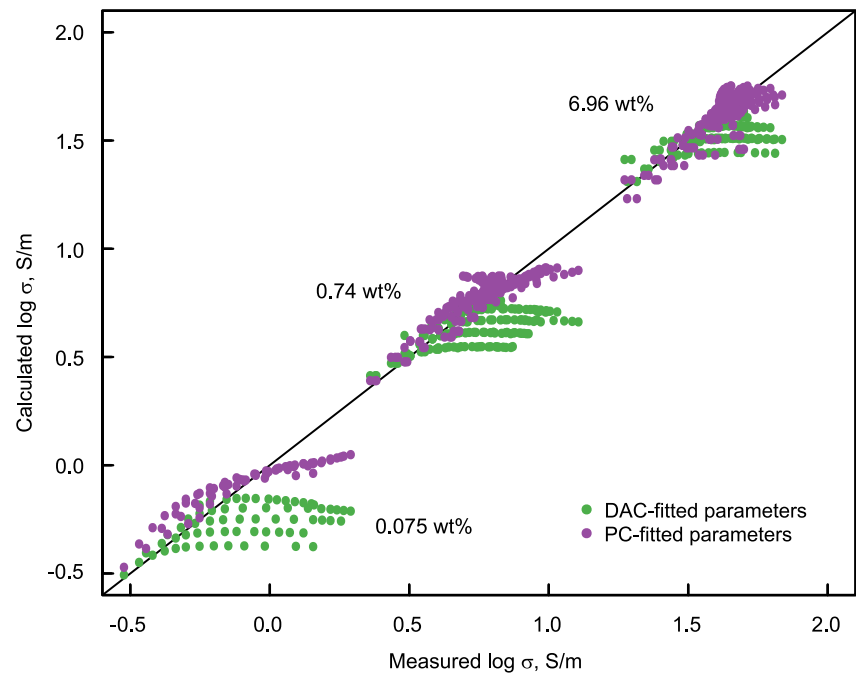
Figure 8. Electrical conductivity of KCl-H$_2$O fluids measured in the piston-cylinder (PC) apparatus and predicted by Equation 5, with fit parameters derived from diamond anvil cell measurements (green) and from PC measurements (purple).

but that difference is normally within ~1 Ω and does not affect the measurement outcome significantly—for any greater difference the experiment was discarded. For 1–2 GPa up to 4 heating-cooling cycles can be performed without any change in the quality of the measured resistances, for 3–5 GPa this number reduces to 3 cycles.

While interpreting our data, we assume that the primary charge carriers in the fluid are K$^+$ and Cl$^-$, produced by KCl dissociation. As previously noted in the NaCl conductivity study by H. Guo and Keppler (2019), at highest pressures and temperatures the auto-dissociation of H$_2$O into H$_3$O$^+$ and OH$^-$ may contribute to measured conductivities in a minor way. As parts of our electrochemical assembly are made of Al$_2$O$_3$ and Au, some contamination from the dissolution of those materials is theoretically possible. However, the solubility of gold in such dilute saline solutions during very short run times (<10 hr of heating per experiment) and their cyclic design is almost negligible (Hanley et al., 2005), with the same being true for the Al$_2$O$_3$. Though no study on corundum solubility in KCl fluid is readily available, the data presented in the study on NaCl (Newton & Manning, 2006) and KOH (Wohlers & Manning, 2009) fluids strongly support that statement.

3.4. Conductivity Model for KCl-Bearing Aqueous Fluids in the Mantle

Our DAC conductivity measurements of H$_2$O-KCl fluids allowed us to establish a model covering a majority of possible crustal conditions. For expanding it to the elevated pressures and temperatures probed by the PC technique, some adjustment is required. Thus, we performed the same least squares fitting procedure on the cleaned PC measurements data set (462 data points), after removing several anomalous single measurements (e.g., KV46 & KV62_3 for temperatures >750°C) where the real experimental conditions may be different from those reported. As previously, limiting molar conductivity values were calculated using Equation 6 with the previously obtained parameter values. A least squares fit ($R^2 = 0.986$) yielded $A = -1.52 \pm 0.02$, $B = -357 \pm 13.4$, $C = 0.865 \pm 0.005$, and $D = 1.72 \pm 0.06$, see Figure 8. For the high-pressure data, the model calibrated by the PC runs clearly reproduces the measurements better. However, the difference between these two models diminishes for elevated KCl concentrations, which are geophysically most relevant. More significant discrepancies between measured and predicted data, most notably for the equation using the fit parameters from the DAC experiments, occur at the lowest KCl concentrations. This is in some ways expected as for such very dilute fluids and in particular for the highest pressures studied here, the solute may approach complete dissociation. In this case, some of the simplifications used by Sinmyo and Keppler (2017) in deriving Equation 5 are not valid anymore.

If one compares the fit coefficients derived from the PC experiments with those from the diamond cell experiments, it is obvious that the coefficient C in front of the concentration term is very similar. However, there is a significant difference in the coefficients D for the density term and a particularly large difference in B, which describes the temperature dependence. This is because the fluid density itself also depends somewhat on temperature and therefore, there is some co-variance between the fit coefficients for the temperature and the fluid density term. At the lower pressures covered by the DAC fit, the effect of temperature on fluid density is much stronger than at the higher pressures covered by the regression fit from the PC data, which causes the difference in B and D. In the 1–2 GPa range, both equations reproduce the data generally well, but the PC calibrated equation should not be used below 1 GPa.

For higher concentrations above 6.96 wt%, we do not have direct experimental data at high temperatures and pressures. Yet Figure 6b suggests that this type of model should provide reasonable results even for 25 wt% solutions, which may justify its use for concentrated brines.

4. Discussion

4.1. Comparison of the Electrical Conductivity of NaCl and KCl-Bearing Fluids

At ambient conditions, 1 M NaCl (5.54 wt%) and 1 M (6.96 wt%) KCl electrical conductivities are 8.5 and 10.9 S/m respectively (Weiner, 1960). This is somewhat surprising, as the ionic radius of Na^+ (0.97 Å) in aqueous solution is less than for K^+ (1.41 Å; Marcus, 1988) and without any additional factors the latter should be less mobile. However, in aqueous solutions, solvation shells are formed around ions. The solvation shell around the potassium ion was traditionally believed to be smaller than the one around sodium, due to the smaller electrostatic field strength (charge/radius ratio) of K^+ (Nightingale, 1959). This concept was used to explain why K^+ is more mobile and more conductive than Na^+ in aqueous solutions at ambient conditions. However, more recent neutron diffraction data (Ohtomo & Arakawa, 1980) suggest that the nearest ion-oxygen distances around Na^+ (2.5 Å) and K^+ (2.7 Å) in aqueous solutions at ambient conditions are similar. The higher conductivity of KCl relative to NaCl at ambient conditions may therefore more be due to weaker interactions between K^+ and H_2O (Džidić & Kebarle, 1970) leading to shorter lifetimes of the associations between K^+ and H_2O molecules (Bakker, 2008). The difference between the conductivity of KCl versus NaCl in aqueous fluids at low pressure and at high pressure may, however, be related to some structural change in the fluid. At low pressure, liquid water has a rather open (ice-like) structure with defined hydration shells around ions (e.g., Ohtomo & Arakawa, 1980). At higher pressures, this structure should break down to a more or less dense packing of oxygen atoms without defined hydration shells. Under these conditions, one would expect KCl to be less conductive than NaCl, because the larger ion (K^+) should move more slowly, consistent with our experimental observations.

Figure 9 compares electrical conductivities of NaCl and KCl-bearing aqueous solutions at elevated pressures and temperatures, calculated with PC-derived parameters from Equation 5 for 6.96 wt% KCl and from H. Guo and Keppler (2019) for 5.54 wt% NaCl. Similar to the situation at ambient conditions, the electrical conductivity of potassium chloride at 1 GPa exceeds that of sodium chloride by approximately a factor of two. However, at higher pressures and temperatures this relation reverses. While NaCl conductivity greatly increases with pressure, the effect on KCl conductivity is small. This may be attributed to a decrease or even loss of hydration shells around the Na^+ and K^+ ions, which may particularly increase sodium mobility as compared to potassium. Although some recent experimental and computational data on Na^+, K^+, and Rb^+ coordination and solvation shell structure at elevated pressure-temperature conditions exist (Filipponi et al., 2003; Rozsa & Galli, 2021; Sakuma & Ichiki, 2016; Yamaguchi et al., 2021), no measurements of the K^+ and Na^+ solvation shells at up to 5 GPa and relevant high temperatures were performed so far. However, a recent theoretical study by Fowler and Sherman (2020) indeed suggests that at high P and T (up to 4.5 GPa and 800°C), the presence of NaCl has essentially no effect on water structure anymore, in agreement with the idea that at these conditions, ordered hydration shells around ions cease to exist.

4.2. KCl-Rich Aqueous Fluid as Possible Electrical Conductor in the Upper Mantle

Highly conductive zones (0.02–1 S/m, see Figures 10 and 11) detected by magnetotelluric surveys in the lithospheric mantle below cratons may be successfully explained by the presence of small (<1 vol%) fractions of various fluids and melts, sulfide minerals, graphite films or hydrous olivine (Naif et al., 2021). Unless there
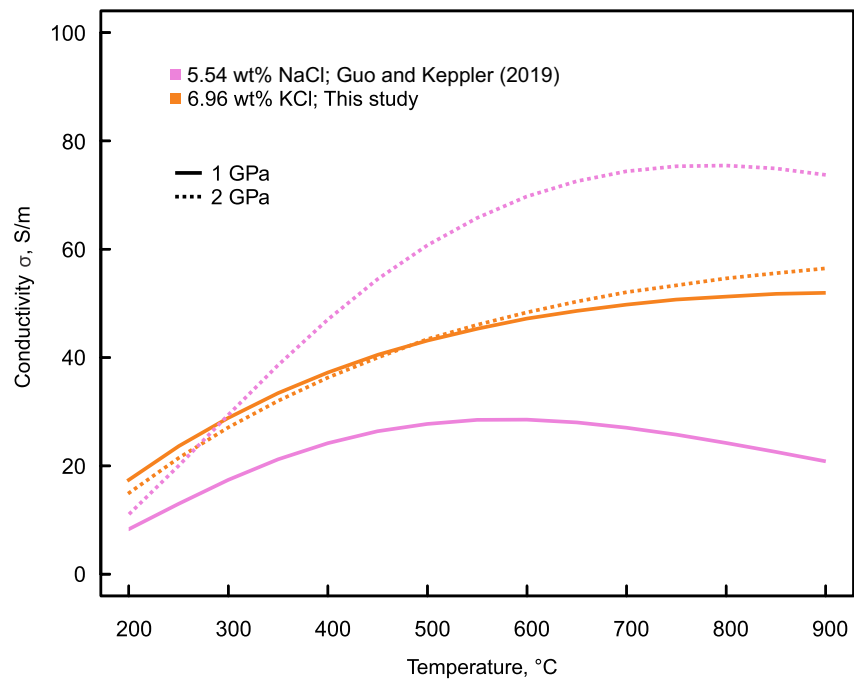
Figure 9. Electrical conductivities of 5.54 wt% (1 M) of NaCl-H$_2$O fluids calculated based on the model of H. Guo and Keppler (2019) and 6.96 wt% KCl-H$_2$O fluid (1M, this study, piston-cylinder model) at 1 and 2 GPa. 1 M refers to a concentration of 1 mol per liter at standard conditions.

is a localized heat source, the low lithospheric mantle temperatures (Hasterok & Chapman, 2011; Rudnick & Fountain, 1995) allow to safely rule out silicate melts and hydrated olivine (Naif et al., 2021). Minimal temperatures of 900–1000°C necessary for the beginning of water-saturated peridotite melting (Katz et al., 2003) are achieved only at depth of 125–150 km (4–5 GPa) with fluids of variable silicate content (Ryabchikov et al., 1982) being present at more shallow depths. Based on a case of sulfide-containing Sierra Nevada xenoliths (Ducea & Park, 2000), an argument for small amount of sulfides as conductivity enhancing phase can be made. Yet there are significant obstacles for a widespread use of this phase for the interpretation of MT data, given it extremely high conductivity on the order of 10^4–10^5 S/m (e.g., Bagdassarov et al., 2009). Similar problems arise when attempting to interpret such conductive anomalies as zones containing graphite (∼10^5 S/m; Frost et al., 1989; Mareschal et al., 1992). Recent studies suggested that carbon films will not form interconnected networks, neither in crust nor in the lithospheric mantle (Yoshino & Noritake, 2011; B. Zhang & Yoshino, 2017), thus making them unlikely candidates. Melts and aqueous fluids, however, typically have conductivities on the order of 10^0–10^2 S/m at upper mantle conditions (Naif et al., 2021 and references within) and do not require improbably large volume fractions to explain the elevated conductivities below cratons. The carbonatite solidus, for example, is located at 500–800°C at 2–5 GPa (Litasov et al., 2013) and hydrous carbonatites have conductivities on the order of 10^1–10^2 S/m along the cratonic geotherm (Yoshino et al., 2018), which makes them a plausible choice as conductive phase. Despite having even lower solidus temperatures (Journaux et al., 2013), higher conductivities (H. Guo & Keppler, 2019), and direct evidence from diamond inclusions, saline aqueous fluids are less frequently considered.

Elevated bulk rock conductivities as inferred by MT data can only be attributed to fluids, if they are interconnected at given conditions (Wannamaker, 2000; Yardley & Valley, 1997). While at lower crustal conditions the presence of fluid is currently debated (Manning, 2018; Naif et al., 2021; Yardley & Valley, 1997), in the upper mantle above 2 GPa and 1000°C (Mibe et al., 1998), aqueous fluids may remain interconnected. Recent work, investigating the connectivity of mixed H$_2$O-NaCl-CO$_2$ fluid in olivine aggregates, demonstrated that for such compositions the fluid is wetting grain boundaries even along a cool geotherm (Huang et al., 2020). Starting from 50 km (1.5–2 GPa) and 750°C, the dihedral angles were experimentally found to be less then 60°.
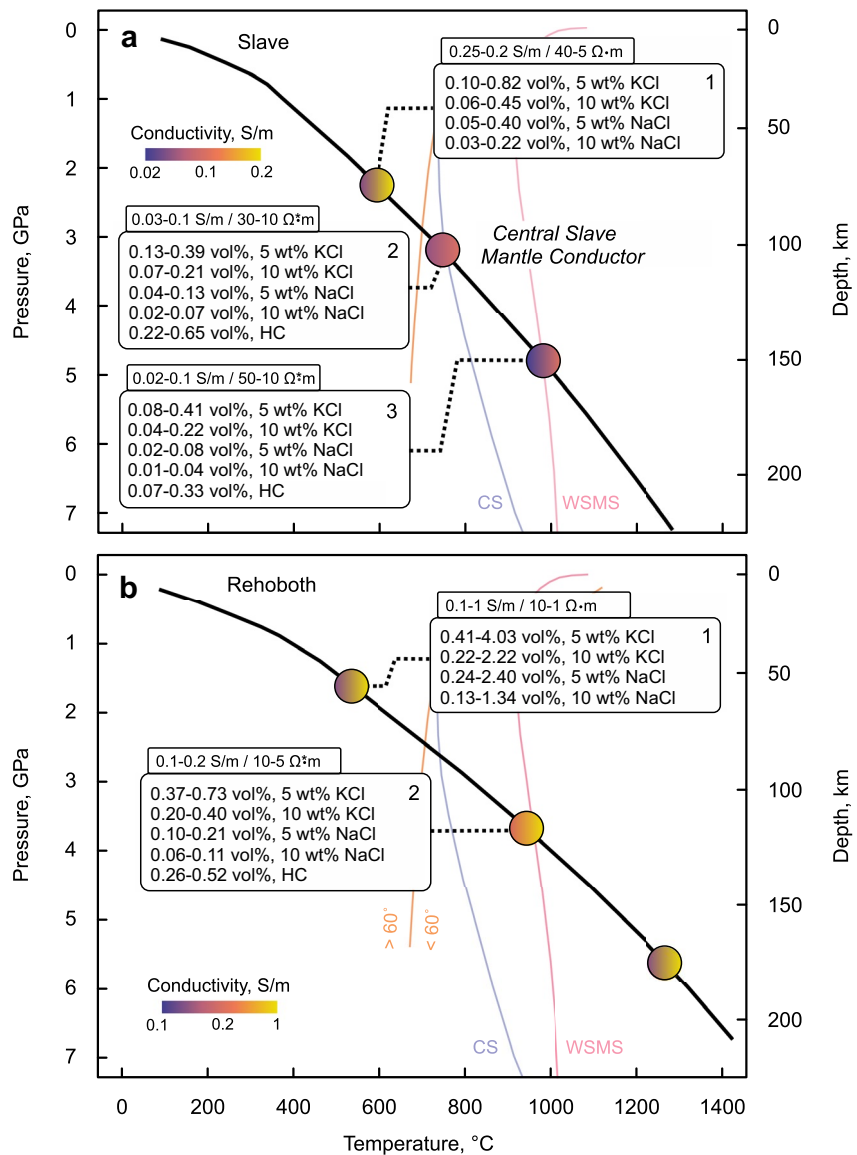
Figure 10. Fractions of various non-silicate fluids, required to explain electrical conductivity anomalies below (a) Slave craton (MT data from Jones et al. [2001, 2003], geotherm from Russell and Kopylova [1999]), (b) Rehoboth terrane and Kaapvaal craton (MT data from Evans et al. [2011] and Jones et al. [2009], geotherm from Rudnick and Nyblade [1999]). Gradients inside the circles on diagrams represent lateral variations in conductivity at given depth at geotherm temperature. HC—hydrous carbonatite melt (Yoshino et al., 2018), CS—coldest possible potassic carbonatite solidus from Litasov et al. (2013), WSMS—water saturated mantle solidus from Katz et al. (2003), the dashed orange line is the 60° dihedral angle isopleth (Huang et al., 2020).

To investigate KCl-rich aqueous fluids as a possible conducting phase in lithospheric mantle of cratons, we calculated possible fluid fractions with Hashin and Shtrikman (1962) upper bound (HS$^+$) model for several known conductive anomalies (Figures 10 and 11) using Equation 5 with PC-fitted set of parameters (exact model values are available in Table S4 of Supporting Information S2). NaCl-bearing fluid (H. Guo & Keppler, 2019) and hydrous carbonatite (Yoshino et al., 2018) fluid fractions are calculated as well for comparison. Peridotite conductivity is estimated from the model of Gardés et al. (2014). Fluid salinities of 5 and 10 wt% were chosen for the model. Frezzotti and Touret (2014) constrain upper mantle fluid salinity at 5–50 wt% in NaCl equivalent, specifying that the lowest values (<15 wt% NaCl eq.) are observed for inclusions with high concentration of CO_2, an prominent component of diamond fluid inclusions. We do not provide estimates for higher salinities on Figure 10, but in general, a salinity increase would almost inversely proportionally decrease the calculated fluid
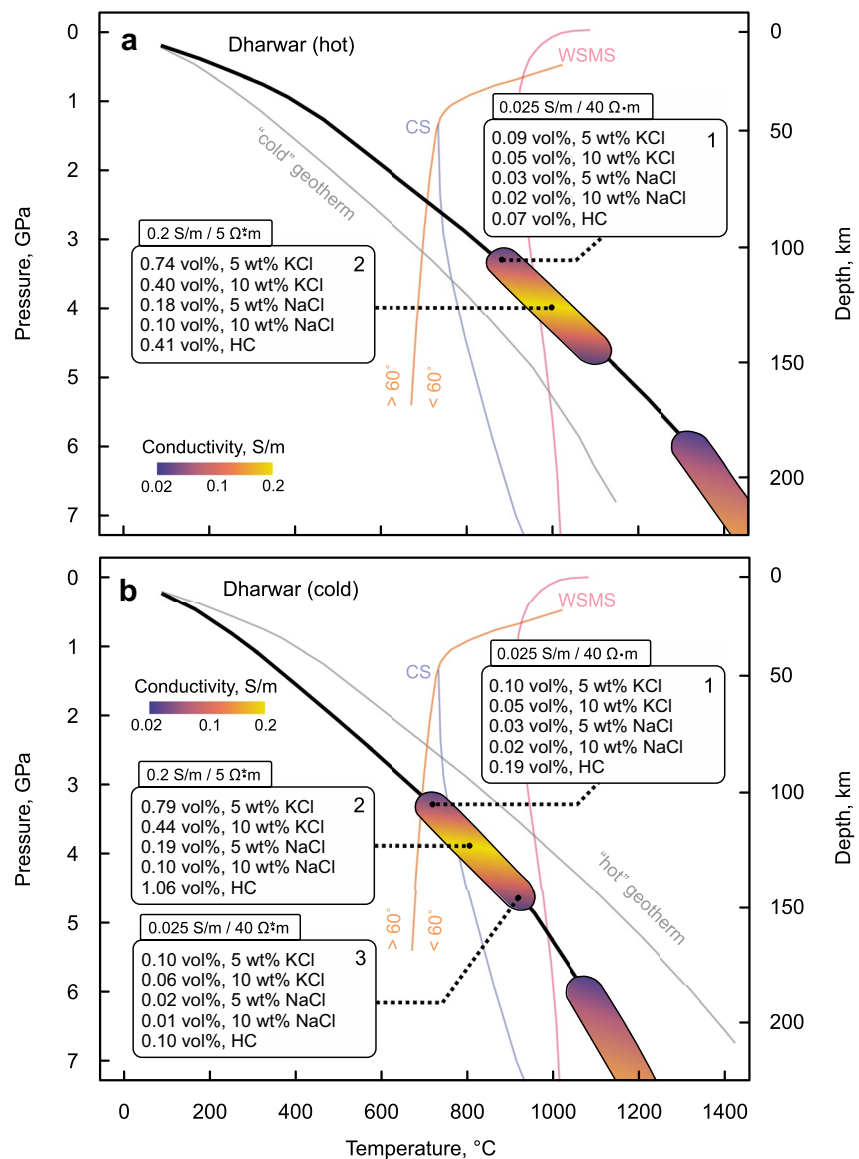
Figure 11. Fractions of various non-silicate fluids, required to explain electrical conductivity anomalies below the Dharwar craton (MT data from Kusham et al. [2018, 2019], with "hot" [Rudnick & Nyblade, 1999]) (a) and "cold" (Gupta et al., 1991) (b) geotherms. Colored areas on diagrams are vertical cross-sections of conductivity anomalies with each shade representing single conductivity value at given depth and temperature. HC—hydrous carbonatite melt (Yoshino et al., 2018), CS— coldest possible potassic carbonatite solidus from Litasov et al. (2013), WSMS—water saturated mantle solidus from Katz et al. (2003), the dashed orange line is the 60° dihedral angle isopleth (Huang et al., 2020).

fraction. As an example, the fluid fraction necessary to explain a 0.03–0.1 S/m mantle conductivity at 3.1 GPa (100 km) and 750°C (Figure 10a, –2) by a 10 wt% NaCl or KCl fluid would be 0.02–0.07 vol% and 0.07–0.21 vol%, while a 20 wt% concentration would require 0.01–0.04 vol% and 0.04–0.12 vol% respectively.

4.3. Conductivity Anomalies in the Lithospheric Mantle of Cratons

As noted in the introduction, there is very good evidence from fluid inclusions in diamonds suggesting the widespread occurrence of KCl-bearing fluids in the cratonic mantle. We will therefore explore here the possible contribution of such fluids to observed zones of elevated conductivities. To qualify as a possible location of KCl-bearing aqueous fluids, a conductive area needs to satisfy several important criteria. (a) The fluid needs to remain interconnected that is, it has to form dihedral angles below 60°. As there are no data for KCl-bearing

fluids, we use the 60° isopleth for NaCl-CO$_2$-H$_2$O from the study of Huang et al. (2020) as the best approximation. (b) The region has to be below the water-saturated mantle solidus. Depending on the geotherm, those two conditions define a narrow window of 700–1000°C and 3–5 GPa or 100–150 km. These considerations effectively exclude some of the deep hot anomalies, shown in Figures 10 and 11 as an example without calculated fluid fractions, and some of the shallower anomalies like Figures 10a and 10b –1. For the extremely conductive zone (>1 S/m) in the Rehoboth terrane, sulfides may perhaps be a plausible explanation, as there is evidence for mantle sulfides from Kaapvaal (Alard et al., 2000). (c) Another criterion, which makes KCl-bearing aqueous fluids a natural choice, is to be below the carbonatite solidus. This criterion defines a region in the lithospheric mantle where such fluids are the most probable choice for explaining elevated conductivities: 3–3.5 GPa below 800°C. This requires a cooler geotherm, as for the Slave craton, where the Central Slave Mantle Conductor (CSMC; Figure 10a –2) is located approximately at those pressures and temperatures. For this particular case, numerous potassic saline fluid inclusions from Panda and Diavik diamonds (see Introduction, Figure 1) provide additional evidence for the presence of KCl-bearing aqueous fluids. The 60° isopleth almost exactly matches the upper border of the CSMC, which is additional evidence for the involvement of aqueous fluid.

In hotter regions of the mantle, KCl-bearing aqueous fluids may also be present. Estimates from Panda inclusions suggest 930–1010°C as diamond formation temperature. However, at those temperatures, carbonatites would also be a plausible option as highly conductive phase. Our calculations suggest that based on conductivities alone a distinction between carbonatites and saline fluids is not possible. Hydrous carbonatites and 5–10 wt% KCl fluids require almost identical fluid fraction at cratonic geotherm conditions (Figures 10 and 11). Interestingly, for the majority of fluid inclusion populations in diamonds, saline HDF coexist with carbonatites (e.g., Klein-BenDavid et al., 2004, 2007; Navon et al., 1988; Schrauder & Navon, 1994) and form a continuous series of intermediate compositions. Therefore, both phases may perhaps contribute to the conductive anomalies.

In general, as illustrated by Figures 10 and 11, accounting for even the most conductive parts of subcratonic upper mantle typically requires less than a volume percent for any of the examined fluids. At the depth below 75 km the most conductive phase is NaCl-rich fluid with the fluid fractions in the order of 10^{-2} vol%. A comparison of saline solution fractions for two Dharwar craton geotherms (Figures 11a and 11b) shows that for both the colder one (Gupta et al., 1991) and the hotter one (Rudnick & Nyblade, 1999), the required volume fractions for KCl and NaCl-bearing aqueous fluids at same depth are very similar, showing little dependence on temperature change within 150°. The fluid fraction required for hydrous carbonatite, for comparison, changes by more than a factor of two—from 1.1 vol% to 0.4 vol%.

The fluid fractions calculated here are based on the conductivity data for pure NaCl-H$_2$O or KCl-H$_2$O fluids. Actual mantle fluids may dissolve some additional silica component and this may increase the viscosity of the fluid and thereby reduce ion mobilities. There is some support for this effect from the comparision of NaCl-H$_2$O fluid conductivity data (Sinmyo & Keppler, 2017) with conductivity data in polyphase systems containing saline fluids (X. Guo et al., 2015; Shimojuku et al., 2014). However, direct viscosity measurements of silica-bearing aqueous fluids suggest only a minor viscosity increase for plausible silica contents in mantle fluids (Audétat & Keppler, 2004). We therefore estimate that our calculated fluid fractions should be accurate within a factor of two.

If saline aqueous fluids are indeed responsible for some of the conductivity anomalies as discussed above, they need to be in some kind of thermodynamic equilibrium with the surrounding mantle assemblage. Moreover, fluid ascent by gravitational instability has to be limited by some mechanism. We propose that there are plausible mechanisms how fluids may be highly connected without being able to ascent rapidly. This is possible if the fluid connectivity is mostly horizontal, with little vertical connectivity. Experimentally, such structures have been produced by deformation in partially molten rocks (Holtzman et al., 2003). Moreover, the wetting properties of olivine are certainly anisotropic and it is therefore conceivable that in a deformed peridotite with lattice preferred orientation of mineral grains, fluid connectivity will also be anisotropic. There are two lines of evidence supporting this idea: (a) Experimental measurements of the dihedral angle in the olivine-H$_2$O-NaCl system suggest values that are rather close to the critical angle of 60°(Huang et al., 2020). But they also show—for the same P, T conditions—a rather wide spread. This is at least partially due to the effects of anisotropy, implying that for some crystal faces, the value may actually below 60°, while it is above 60° for other crystal faces under the same conditions. A lattice preferred orientation of olivine crystals in the mantle could therefore very well produce fluid connectivity only in one (e.g., horizontal) direction. (b) Seismic data provide strong evidence for the presence of small degrees of partial melt in the form of tubes or thin films of nearly horizontal

orientation near the lithosphere-asthenosphere boundary (e.g., Rychert et al., 2021). The stabilization of such connected melt structures over geologic timescales poses the same problems as for fluids as it requires that the vertical connectivity and the buoyant ascent of the melt has to be somehow reduced or suppressed. The lattice preferred orientation of olivine and other mantle minerals, as it results from mantle convection, together with the anisotropy of wetting properties could offer here a plausible explanation. An alternative possibility could be that aqueous fluid is constrained to depths where it forms an interconnected network and it cannot acent any further, because the wetting properties of the fluid become unfavorable at low pressures corresponding to more shallow depths. Indeed, the data of Huang et al. (2020) suggest that for NaCl-bearing fluids, such a change in connectivity occurs in the shallow mantle (see the orange line in Figure 11). However, the intersection of this line with the geotherm (Figure 11) is not always at the right depth for stabilizing a fluid in the region where elevated conductivity is observed.

Thermodynamic equilibrium between a saline fluid and the nominally anhydrous minerals of the upper mantle is also possible, if one considers that in such a fluid the activity of water may be greatly reduced. The $NaCl-H_2O$ system at high pressure has a strong negative deviation from ideality, which increases with pressure, as the degree of dissociation of NaCl increases (e.g., Manning & Aranovich, 2014). For KCl, which is more dissociated than NaCl, this effect should be even stronger. Moreover, at mantle pressures and temperatures, the solubility of silicate species in the water is very significant, which further reduces water activity. Both effects together will tend to destabilize hydrous phases and reduce water solubility in nominally anhydrous minerals, such that a saline fluid containing some dissolved silicates may well be in stable equilibrium with a mostly anhydrous mantle assemblage. Moreover, the bulk water content of conductive mantle regions may well be elevated above average bulk mantle water contents. This is completely consistent with data on water contents in mantle xenoliths, which show quite a large regional variation (e.g., Demouchy & Bolfan-Casanova, 2016).

5. Conclusion

In this paper, we present improvements to previously proposed high-temperature—high-pressure electrochemical cells, allowing more accurate electrical conductivity measurements, as well as a detailed equivalent circuit that allows to interpret such data. Based on those methodological developments we investigated the electrical conductivities of $KCl-H_2O$ fluids and proposed two conductivity models: one for crustal conditions (to 2.5 GPa and 675°C) and one for the upper mantle (to 5 GPa and 900°C). Using these models, we interpreted a class of known lithospheric mantle conductive anomalies as possible zones containing traces of KCl-bearing fluid. Comparing our data with previously measured conductivities of NaCl -bearing aqueous fluids reveals that at high pressures and temperatures NaCl-bearing fluid of same molality is significantly more conductive than KCl-bearing. This may be caused by major changes in the hydration shell structure.

Data Availability Statement

All research data for this manuscript is provided in supporting information and also available on figshare (https://doi.org/10.6084/m9.figshare.18551303.v1).

References

Alard, O., Griffin, W. L., Lorand, J. P., Jackson, S. E., & O'Reilly, S. Y. (2000). Non-chondritic distribution of the highly siderophile elements in mantle sulphides. *Nature*, *407*(6806), 891–894. https://doi.org/10.1038/35038049

Audétat, A., & Keppler, H. (2004). Viscosity of fluids in subduction zones. *Science*, *303*(5657), 513–516. https://doi.org/10.1126/science.1092282

Bagdassarov, N., Golabek, G. J., Solferino, G., & Schmidt, M. W. (2009). Constraints on the Fe-S melt connectivity in mantle silicates from electrical impedance measurements. *Physics of the Earth and Planetary Interiors*, *177*(3–4), 139–146. https://doi.org/10.1016/j.pepi.2009.08.003

Bakker, H. J. (2008). Structural dynamics of aqueous salt solutions. *Chemical Reviews*, *108*, 1456–1473. https://doi.org/10.1021/cr0206622

Barsoukov, E., & Macdonald, J. R. (2005). Impedance spectroscopy: Theory, experiment, and applications. In E. Barsoukov & J. R. Macdonald (Eds.), *Impedance spectroscopy: Theory, experiment, and applications*. Wiley. https://doi.org/10.1002/0471716243

Bassett, W. A., Shen, A. H., Bucknum, M., & Chou, I. M. (1993). A new diamond anvil cell for hydrothermal studies to 2.5 GPa and from −190 to 1200°C. *Review of Scientific Instruments*, *64*(8), 2340–2345. https://doi.org/10.1063/1.1143931

Bose, K., & Ganguly, J. (1995). Quartz-coesite transition revisited: Reversed experimental determination at 500–1200°C and retrieved thermochemical properties. *American Mineralogist*, *80*(3–4), 231–238. https://doi.org/10.2138/am-1995-3-404

Burgess, R., Cartigny, P., Harrison, D., Hobson, E., & Harris, J. (2009). Volatile composition of microinclusions in diamonds from the Panda kimberlite, Canada: Implications for chemical and isotopic heterogeneity in the mantle. *Geochimica et Cosmochimica Acta*, *73*(6), 1779–1794. https://doi.org/10.1016/j.gca.2008.12.025

Corti, H. R. (2008). Electrical conductivity in hydrothermal binary and ternary systems. In *Hydrothermal Properties of Materials* (pp. 207–226). John Wiley & Sons. https://doi.org/10.1002/9780470094679.ch4

Dawson, J. B. (2012). *Kimberlites and their xenoliths* (Vol. 15). Springer Science & Business Media.

Demouchy, S., & Bolfan-Casanova, N. (2016). Distribution and transport of hydrogen in the lithospheric mantle: A review. *Lithos*, *240–243*, 402–425. https://doi.org/10.1016/j.lithos.2015.11.012

Dobrzhinetskaya, L. F., Wirth, R., & Green, H. W. (2005). Direct observation and analysis of a trapped COH fluid growth medium in metamorphic diamond. *Terra Nova*, *17*(5), 472–477. https://doi.org/10.1111/j.1365-3121.2005.00635.x

Ducea, M. N., & Park, S. K. (2000). Enhanced mantle conductivity from sulfide minerals, southern Sierra Nevada, California. *Geophysical Research Letters*, *27*(16), 2405–2408. https://doi.org/10.1029/2000GL011565

Džidić, I., & Kebarle, P. (1970). Hydration of the alkali ions in the gas phase. Enthalpies and entropies of reaction $M^+(H_2O)_{n-1} + H_2O = M^+(H_2O)_n$. *The Journal of Physical Chemistry*, *74*(7), 1466–1474. https://doi.org/10.1021/j100702a013

Evans, R. L., Jones, A. G., Garcia, X., Muller, M., Hamilton, M., Evans, S., et al. (2011). Electrical lithosphere beneath the Kaapvaal craton, southern Africa. *Journal of Geophysical Research*, *116*(4), 4105. https://doi.org/10.1029/2010JB007883

Evans, R. L., Wannamaker, P. E., McGary, R. S., & Elsenbeck, J. (2014). Electrical structure of the central Cascadia subduction zone: The EMSLAB Lincoln Line revisited. *Earth and Planetary Science Letters*, *402*, 265–274. https://doi.org/10.1016/j.epsl.2013.04.021

Filipponi, A., De Panfilis, S., Oliva, C., Ricci, M. A., D'Angelo, P., & Bowron, D. T. (2003). Ion hydration under pressure. *Physical Review Letters*, *91*(16), 165505. https://doi.org/10.1103/PhysRevLett.91.165505

Fowler, S. J., & Sherman, D. M. (2020). The nature of NaCl–H_2O deep fluids from ab initio molecular dynamics at 0.5–4.5 GPa, 20–800°C, and 1–14 m NaCl. *Geochimica et Cosmochimica Acta*, *277*, 243–264. https://doi.org/10.1016/j.gca.2020.03.031

Frezzotti, M. L., & Ferrando, S. (2018). *The role of halogens in the lithospheric mantle* (pp. 805–845). Springer. https://doi.org/10.1007/978-3-319-61667-4_13

Frezzotti, M. L., Ferrando, S., Tecce, F., & Castelli, D. (2012). Water content and nature of solutes in shallow-mantle fluids from fluid inclusions. *Earth and Planetary Science Letters*, *351–352*, 70–83. https://doi.org/10.1016/j.epsl.2012.07.023

Frezzotti, M. L., & Touret, J. L. R. (2014). CO_2, carbonate-rich melts, and brines in the mantle. *Geoscience Frontiers*, *5*(5), 697–710. https://doi.org/10.1016/j.gsf.2014.03.014

Frost, B. R., Fyfe, W. S., Tazaki, K., & Chan, T. (1989). Grain boundary graphite in rocks and implications for high electrical conductivity. *Nature*, *340*(6229), 134–136. https://doi.org/10.1038/340134a0

Gardés, E., Gaillard, F., & Tarits, P. (2014). Toward a unified hydrous olivine electrical conductivity law. *Geochemistry, Geophysics, Geosystems*, *15*(12), 4984–5000. https://doi.org/10.1002/2014GC005496

Guo, H., & Keppler, H. (2019). Electrical conductivity of NaCl-bearing aqueous fluids to 900°C and 5 GPa. *Journal of Geophysical Research: Solid Earth*, *124*, 1397–1411. https://doi.org/10.1029/2018jb016658

Guo, X., Yoshino, T., & Shimojuku, A. (2015). Electrical conductivity of albite–(quartz)–water and albite–water–NaCl systems and its implication to the high conductivity anomalies in the continental crust. *Earth and Planetary Science Letters*, *412*, 1–9. https://doi.org/10.1016/j.epsl.2014.12.021

Gupta, M. L., Sundar, A., & Sharma, S. R. (1991). Heat flow and heat generation in the Archaean Dharwar cratons and implications for the Southern Indian Shield geotherm and lithospheric thickness. *Tectonophysics*, *194*(1–2), 107–122. https://doi.org/10.1016/0040-1951(91)90275-W

Hanley, J. J., Pettke, T., Mungall, J. E., & Spooner, E. T. C. (2005). The solubility of platinum and gold in NaCl brines at 1.5 kbar, 600 to 800°C: A laser ablation ICP-MS pilot study of synthetic fluid inclusions. *Geochimica et Cosmochimica Acta*, *69*(10), 2593–2611. https://doi.org/10.1016/j.gca.2004.11.005

Hashin, Z., & Shtrikman, S. (1962). A variational approach to the theory of the effective magnetic permeability of multiphase materials. *Journal of Applied Physics*, *33*(10), 3125–3131. https://doi.org/10.1063/1.1728579

Hasterok, D., & Chapman, D. S. (2011). Heat production and geotherms for the continental lithosphere. *Earth and Planetary Science Letters*, *307*(1–2), 59–70. https://doi.org/10.1016/j.epsl.2011.04.034

Ho, P. C., & Palmer, D. A. (1997). Ion association of dilute aqueous potassium chloride and potassium hydroxide solutions to 600°C and 300 MPa determined by electrical conductance measurements. *Geochimica et Cosmochimica Acta*, *61*(15), 3027–3040. https://doi.org/10.1016/S0016-7037(97)00146-4

Holtzman, B. K., Groebner, N. J., Zimmerman, M. E., Ginsberg, S. B., & Kohlstedt, D. L. (2003). Stress-driven melt segregation in partially molten rocks. *Geochemistry, Geophysics, Geosystems*, *4*(5). https://doi.org/10.1029/2001GC000258

Huang, Y., Nakatani, T., Nakamura, M., & McCammon, C. (2020). Experimental constraint on grain-scale fluid connectivity in subduction zones. *Earth and Planetary Science Letters*, *552*, 116610. https://doi.org/10.1016/j.epsl.2020.116610

Hwang, J. U., Lüdemann, H. D., & Hartmann, D. (1970). Die elektrische Leitfahigkeit konzentrierter wassriger Alkalihalogenidlosungen bei hohen Drucken und Temperaturen. *High Temperatures-High Pressures*, *2*, 651–669.

Hwang, S. L., Shen, P., Chu, H. T., Yui, T. F., Liou, J. G., Sobolev, N. V., & Shatsky, V. S. (2005). Crust-derived potassic fluid in metamorphic microdiamond. *Earth and Planetary Science Letters*, *231*(3–4), 295–306. https://doi.org/10.1016/j.epsl.2005.01.002

Irifune, T., Kurio, A., Sakamoto, S., Inoue, T., & Sumiya, H. (2003). Materials: Ultrahard polycrystalline diamond from graphite. *Nature*, *421*(6923), 599–600. https://doi.org/10.1038/421599b

Izraeli, E. S., Harris, J. W., & Navon, O. (2001). Brine inclusions in diamonds: A new upper mantle fluid. *Earth and Planetary Science Letters*, *187*(3–4), 323–332. https://doi.org/10.1016/S0012-821X(01)00291-6

Izraeli, E. S., Harris, J. W., & Navon, O. (2004). Fluid and mineral inclusions in cloudy diamonds from Koffiefontein, South Africa. *Geochimica et Cosmochimica Acta*, *68*(11), 2561–2575. https://doi.org/10.1016/j.gca.2003.09.005

Jones, A. G., Evans, R. L., Muller, M. R., Hamilton, M. P., Miensopust, M. P., Garcia, X., et al. (2009). Area selection for diamonds using magnetotellurics: Examples from southern Africa. *Lithos*, *112*, 83–92. https://doi.org/10.1016/j.lithos.2009.06.011

Jones, A. G., Ferguson, I. J., Chave, A. D., Evans, R. L., & McNeice, G. W. (2001). Electric lithosphere of the Slave craton. *Geology*, *29*(5), 423–426. https://doi.org/10.1130/0091-7613(2001)029<0423:ELOTSC>2.0.CO;2

Jones, A. G., Lezaeta, P., Ferguson, I. J., Chave, A. D., Evans, R. L., Garcia, X., & Spratt, J. (2003). The electrical structure of the Slave craton. *Lithos*, *71*(2–4), 505–527. https://doi.org/10.1016/j.lithos.2003.08.001

Journaux, B., Daniel, I., Caracas, R., Montagnac, G., & Cardon, H. (2013). Influence of NaCl on ice VI and ice VII melting curves up to 6 GPa, implications for large icy moons. *Icarus*, *226*(1), 355–363. https://doi.org/10.1016/j.icarus.2013.05.039

Katz, R. F., Spiegelman, M., & Langmuir, C. H. (2003). A new parameterization of hydrous mantle melting. *Geochemistry, Geophysics, Geosystems*, *4*(9). https://doi.org/10.1029/2002GC000433

Klein-BenDavid, O., Izraeli, E. S., Hauri, E., & Navon, O. (2004). Mantle fluid evolution—A tale of one diamond. *Lithos*, *77*(1–4), 243–253. https://doi.org/10.1016/j.lithos.2004.04.003

Klein-BenDavid, O., Izraeli, E. S., Hauri, E., & Navon, O. (2007). Fluid inclusions in diamonds from the Diavik mine, Canada and the evolution of diamond-forming fluids. *Geochimica et Cosmochimica Acta*, *71*(3), 723–744. https://doi.org/10.1016/j.gca.2006.10.008

Konzett, J., Wirth, R., Hauzenberger, C., & Whitehouse, M. (2013). Two episodes of fluid migration in the Kaapvaal Craton lithospheric mantle associated with Cretaceous kimberlite activity: Evidence from a harzburgite containing a unique assemblage of metasomatic zirconium-phases. *Lithos*, *182–183*, 165–184. https://doi.org/10.1016/j.lithos.2013.10.005

Kusham, Naick, B. P., Pratap, A., & Naganjaneyulu, K. (2021). Magnetotelluric 3-D full tensor inversion in the Dharwar craton, India: Mapping of subduction polarity and kimberlitic melt. *Physics of the Earth and Planetary Interiors*, *315*, 106708. https://doi.org/10.1016/j.pepi.2021.106708

Kusham, Pratap, A., Naick, B. P., & Naganjaneyulu, K. (2018). Lithospheric architecture in the Archaean Dharwar craton, India: A magnetotelluric model. *Journal of Asian Earth Sciences*, *163*, 43–53. https://doi.org/10.1016/j.jseaes.2018.05.022

Kusham, Pratap, A., Naick, B. P., & Naganjaneyulu, K. (2019). Crustal and lithospheric mantle conductivity structure in the Dharwar craton, India. *Journal of Asian Earth Sciences*, *176*, 253–263. https://doi.org/10.1016/j.jseaes.2019.02.015

Litasov, K. D., Shatskiy, A., Ohtani, E., & Yaxley, G. M. (2013). Solidus of alkaline carbonatite in the deep mantle. *Geology*, *41*(1), 79–82. https://doi.org/10.1130/G33488.1

Lussier, A., Ball, N. A., Hawthorne, F. C., Henry, D. J., Shimizu, R., Ogasawara, Y., & Ota, T. (2016). Maruyamaite, $K(MgAl_2)(Al_5Mg)$ $Si_6O_{18}(BO_3)_3(OH)_3O$, a potassium-dominant tourmaline from the ultrahigh-pressure Kokchetav massif, northern Kazakhstan: Description and crystal structure. *American Mineralogist*, *101*(2), 355–361. https://doi.org/10.2138/am-2016-5359

Lvovich, V. F. (2015). *Impedance spectroscopy: Applications to electrochemical and dielectric phenomena. Impedance spectroscopy: Applications to electrochemical and dielectric phenomena*. John Wiley & Sons, Inc. https://doi.org/10.1002/9781118164075

Mangold, K., & Franck, E. U. (1969). Elektrische Leitfähigkeit wäßriger Lösungen bei hohen Temperaturen und Drucken. II [1]. Alkalichloride in Wasser bis 1000°C und 12 kbar. *Berichte der Bunsen-Gesellschaft für Physikalische Chemie*, *73*(1), 21–27. https://doi.org/10.1002/BBPC.19690730107

Manning, C. E. (2018). Fluids of the lower crust: Deep is different. *Annual Review of Earth and Planetary Sciences*, *46*(1), 67–97. https://doi.org/10.1146/annurev-earth-060614-105224

Manning, C. E., & Aranovich, L. Y. (2014). Brines at high pressure and temperature: Thermodynamic, petrologic and geochemical effects. *Precambrian Research*, *253*, 6–16. https://doi.org/10.1016/j.precamres.2014.06.025

Marcus, Y. (1988). Ionic radii in aqueous solutions. *Chemical Reviews*, *88*(8), 1475–1498. https://doi.org/10.1021/cr00090a003

Mareschal, M., Fyfe, W. S., Percival, J., & Chan, T. (1992). Grain-boundary graphite in Kapuskasing gneisses and implications for lower-crustal conductivity. *Nature*, *357*(6380), 674–676. https://doi.org/10.1038/357674a0

Marshall, W., & Frantz, J. D. (1987). Electrical conductance measurement of dilute, aqueous electrolytes at temperatures to 800°C and pressures to 4000 bars: Techniques and Interpretations. In G. Ulmer & H. Barnes (Eds.), *Hydrothermal and experimental techniques* (pp. 261–292). Wiley-Interscience.

Mibe, K., Fujii, T., & Yasuda, A. (1998). Connectivity of aqueous fluid in the Earth's upper mantle. *Geophysical Research Letters*, *25*(8), 1233–1236. https://doi.org/10.1029/98GL00872

Mikhno, A. O., Schmidt, U., & Korsakov, A. V. (2014). Origin of K-cymrite and kokchetavite in the polyphase mineral inclusions from Kokchetav UHP calc-silicate rocks: Evidence from confocal Raman imaging. *European Journal of Mineralogy*, *25*(5), 807–816. https://doi.org/10.1127/0935-1221/2013/0025-2321

Naif, S., Selway, K., Murphy, B. S., Egbert, G., & Pommier, A. (2021). Electrical conductivity of the lithosphere-asthenosphere system. *Physics of the Earth and Planetary Interiors*, *313*, 106661. https://doi.org/10.1016/j.pepi.2021.106661

Navon, O., Hutcheon, I. D., Rossman, G. R., & Wasserburg, G. J. (1988). Mantle-derived fluids in diamond micro-inclusions. *Nature*, *335*(6193), 784–789. https://doi.org/10.1038/335784a0

Newton, R. C., & Manning, C. E. (2006). Solubilities of corundum, wollastonite and quartz in H_2O-NaCl solutions at 800°C and 10 kbar: Interaction of simple minerals with brines at high pressure and temperature. *Geochimica et Cosmochimica Acta*, *70*(22), 5571–5582. https://doi.org/10.1016/j.gca.2006.08.012

Ni, H., Chen, Q., & Keppler, H. (2014). Electrical conductivity measurements of aqueous fluids under pressure with a hydrothermal diamond anvil cell. *Review of Scientific Instruments*, *85*(11), 115107. https://doi.org/10.1063/1.4902152

Ni, H., Keppler, H., & Behrens, H. (2011). Electrical conductivity of hydrous basaltic melts: Implications for partial melting in the upper mantle. *Contributions to Mineralogy and Petrology*, *162*(3), 637–650. https://doi.org/10.1007/s00410-011-0617-4

Ni, H., Keppler, H., Manthilake, M. A. G. M., & Katsura, T. (2011). Electrical conductivity of dry and hydrous $NaAlSi_3O_8$ glasses and liquids at high pressures. *Contributions to Mineralogy and Petrology*, *162*(3), 501–513. https://doi.org/10.1007/s00410-011-0608-5

Nightingale, E. R. (1959). Phenomenological theory of ion solvation. Effective radii of hydrated ions. *Journal of Physical Chemistry*, *63*(9), 1381–1387. https://doi.org/10.1021/j150579a011

Ohtomo, N., & Arakawa, K. (1980). Neutron diffraction study of aqueous ionic solutions. II. Aqueous solutions of sodium chloride and potassium chloride. *Bulletin of the Chemical Society of Japan*, *53*(7), 1789–1794. https://doi.org/10.1246/bcsj.53.1789

O'Reilly, S. Y., & Griffin, W. L. (2013). Mantle metasomatism. In *Lecture Notes in Earth system Sciences* (pp. 471–533). Springer International Publishing. https://doi.org/10.1007/978-3-642-28394-9_12

Patkó, L., Novák, A., Klébesz, R., Liptai, N., Lange, T. P., Molnár, G., et al. (2021). Effect of metasomatism on the electrical resistivity of the lithospheric mantle – An integrated research using magnetotelluric sounding and xenoliths beneath the Nógrád-Gömör Volcanic Field. *Global and Planetary Change*, *197*, 103389. https://doi.org/10.1016/j.gloplacha.2020.103389

Pommier, A. (2014). Interpretation of magnetotelluric results using laboratory measurements. *Surveys in Geophysics*, *35*(1), 41–84. https://doi.org/10.1007/s10712-013-9226-2

Pommier, A., & Evans, R. L. (2017). Constraints on fluids in subduction zones from electromagnetic data. *Geosphere*, *13*(4), 1026–1041. https://doi.org/10.1130/GES01473.1

Quist, A. S., & Marshall, W. L. (1968). Electrical conductances of aqueous sodium chloride solutions from 0 to 800° and at pressures to 4000 bars. *The Journal of Physical Chemistry*, *72*(2), 684–703. https://doi.org/10.1021/j100848a050

Randles, J. E. B. (1947). Kinetics of rapid electrode reactions. *Discussions of the Faraday Society*, *1*, 11–19. https://doi.org/10.1039/DF9470100011

Rege, S., Griffin, W. L., Pearson, N. J., Araujo, D., Zedgenizov, D., & O'Reilly, S. Y. (2010). Trace-element patterns of fibrous and monocrystalline diamonds: Insights into mantle fluids. *Lithos*, *118*(3–4), 313–337. https://doi.org/10.1016/j.lithos.2010.05.007

Ritzert, G., & Franck, E. U. (1968). Elektrische Leitfähigkeit wäßriger Lösungen bei hohen Temperaturen und Drucken. I KCl, $BaCl_2$, $Ba(OH)_2$ und $MgSO_4$ bis 750°C und 6 kbar. *Berichte der Bunsen-Gesellschaft für Physikalische Chemie*, *72*(7), 798–808. https://doi.org/10.1002/bbpc.19680720712

Rozsa, V., & Galli, G. (2021). Solvation of simple ions in water at extreme conditions. *Journal of Chemical Physics*, *154*(14), 144501. https://doi.org/10.1063/5.0046193

Rudnick, R. L., & Fountain, D. M. (1995). Nature and composition of the continental crust: A lower crustal perspective. *Reviews of Geophysics*, *33*(3), 267–309. https://doi.org/10.1029/95RG01302

Rudnick, R. L., & Nyblade, A. A. (1999). The thickness and heat production of Archean lithosphere: Constraints from xenolith thermobarometry and surface heat flow. *Mantle Petrology: Field Observations and High Pressure Experimentation: A Tribute to Francis R.(Joe) Boyd*, *6*, 3–12.

Russell, J. K., & Kopylova, M. G. (1999). A steady state conductive geotherm for the north central Slave, Canada: Inversion of petrological data from the Jericho Kimberlite pipe. *Journal of Geophysical Research*, *104*(B4), 7089–7101. https://doi.org/10.1029/1999jb900012

Ryabchikov, I. D., Schreyer, W., & Abraham, K. (1982). Compositions of aqueous fluids in equilibrium with pyroxenes and olivines at mantle pressures and temperatures. *Contributions to Mineralogy and Petrology*, *79*(1), 80–84. https://doi.org/10.1007/BF00376964

Rychert, C. A., Tharimena, S., Harmon, N., Wang, S., Constable, S., Kendall, J. M., et al. (2021). A dynamic lithosphere–asthenosphere boundary near the equatorial Mid-Atlantic Ridge. *Earth and Planetary Science Letters*, *566*, 116949. https://doi.org/10.1016/j.epsl.2021.116949

Sakuma, H., & Ichiki, M. (2016). Electrical conductivity of NaCl-H_2O fluid in the crust. *Journal of Geophysical Research: Solid Earth*, *121*(2), 577–594. https://doi.org/10.1002/2015JB012219

Savova-Stoynov, B., & Stoynov, Z. B. (1987). Analysis of the inductance influence on the measured electrochemical impedance. *Journal of Applied Electrochemistry*, *17*(6), 1150–1158. https://doi.org/10.1007/BF01023598

Schertl, H. P., & Sobolev, N. V. (2013). The Kokchetav Massif, Kazakhstan: "Type locality" of diamond-bearing UHP metamorphic rocks. *Journal of Asian Earth Sciences*, *63*, 5–38. https://doi.org/10.1016/j.jseaes.2012.10.032

Schmidt, C., Steele-MacInnis, M., Watenphul, A., & Wilke, M. (2013). Calibration of zircon as a Raman spectroscopic pressure sensor to high temperatures and application to water-silicate melt systems. *American Mineralogist*, *98*(4), 643–650. https://doi.org/10.2138/am.2013.4143

Schrauder, M., Koeberl, C., & Navon, O. (1996). Trace element analyses of fluid-bearing diamonds from Jwaneng, Botswana. *Geochimica et Cosmochimica Acta*, *60*(23), 4711–4724. https://doi.org/10.1016/S0016-7037(96)00274-8

Schrauder, M., & Navon, O. (1994). Hydrous and carbonatitic mantle fluids in fibrous diamonds from Jwaneng, Botswana. *Geochimica et Cosmochimica Acta*, *58*(2), 761–771. https://doi.org/10.1016/0016-7037(94)90504-5

Seno, T., & Rehman, H. U. (2011). When and why the continental crust is subducted: Examples of Hindu Kush and Burma. *Gondwana Research*, *19*(1), 327–333. https://doi.org/10.1016/j.gr.2010.05.011

Sharygin, A. V., Wood, R. H., Zimmerman, G. H., & Balashov, V. N. (2002). Multiple ion association versus redissociation in aqueous NaCl and KCl at high temperatures. *Journal of Physical Chemistry B*, *106*(28), 7121–7134. https://doi.org/10.1021/jp013647uCCC:22.00

Shimojuku, A., Yoshino, T., & Yamazaki, D. (2014). Electrical conductivity of brine-bearing quartzite at 1 GPa: Implications for fluid content and salinity of the crust. *Earth, Planets and Space*, *66*(1), 2. https://doi.org/10.1186/1880-5981-66-2

Sinmyo, R., & Keppler, H. (2017). Electrical conductivity of NaCl-bearing aqueous fluids to 600°C and 1 GPa. *Contributions to Mineralogy and Petrology*, *172*(1), 4. https://doi.org/10.1007/s00410-016-1323-z

Smith, E. M., Kopylova, M. G., Nowell, G. M., Graham Pearson, D., & Ryder, J. (2012). Archean mantle fluids preserved in fibrous diamonds from Wawa, Superior craton. *Geology*, *40*(12), 1071–1074. https://doi.org/10.1130/G33231.1

Tomlinson, E. L., Jones, A. P., & Harris, J. W. (2006). Co-existing fluid and silicate inclusions in mantle diamond. *Earth and Planetary Science Letters*, *250*(3–4), 581–595. https://doi.org/10.1016/j.epsl.2006.08.005

Tomlinson, E. L., & Müller, W. (2009). A snapshot of mantle metasomatism: Trace element analysis of coexisting fluid (LA-ICP-MS) and silicate (SIMS) inclusions in fibrous diamonds. *Earth and Planetary Science Letters*, *279*(3–4), 362–372. https://doi.org/10.1016/j.epsl.2009.01.010

Vandersande, J. W., & Zoltan, L. D. (1991). High temperature electrical conductivity measurements of natural diamond and diamond films. *Surface and Coatings Technology*, *47*(1–3), 392–400. https://doi.org/10.1016/0257-8972(91)90305-G

Wagner, W., & Pruß, A. (2002). The IAPWS formulation 1995 for the thermodynamic properties of ordinary water substance for general and scientific use. *Journal of Physical and Chemical Reference Data*, *31*(2), 387–535. https://doi.org/10.1063/1.1461829

Wannamaker, P. E. (2000). Comment on "The petrologic case for a dry lower crust" by Bruce W. D. Yardley and John W. Valley. *Journal of Geophysical Research*, *105*(B3), 6057–6064. https://doi.org/10.1029/1999JB900324

Weiner, R. (1960). *R. Parsons: Handbook of electrochemical constants*. Butterworths Scientific Publications. Preis: s. 30./- net. Zeitschrift Für Elektrochemie, Berichte Der Bunsengesellschaft Für Physikalische Chemie, 64(6), 872–873. https://doi.org/10.1002/BBPC.19600640623

Weiss, Y., & Goldstein, S. L. (2018). The involvement of diamond-forming fluids in the metasomatic 'cocktail' of kimberlite sources. *Mineralogy and Petrology*, *112*(1), 149–167. https://doi.org/10.1007/s00710-018-0613-8

Weiss, Y., Kiflawi, I., Davies, N., & Navon, O. (2014). High-density fluids and the growth of monocrystalline diamonds. *Geochimica et Cosmochimica Acta*, *141*, 145–159. https://doi.org/10.1016/j.gca.2014.05.050

Wohlers, A., & Manning, C. E. (2009). Solubility of corundum in aqueous KOH solutions at 700°C and 1 GPa. *Chemical Geology*, *262*(3–4), 310–317. https://doi.org/10.1016/j.chemgeo.2009.01.025

Wu, Y. C., Koch, W. F., & Pratt, K. W. (1991). Proposed new electrolytic conductivity primary standards for KCl solutions. *Journal of Research of the National Institute of Standards and Technology*, *96*(2), 191. https://doi.org/10.6028/jres.096.008

Yamaguchi, T., Fukuyama, N., Yoshida, K., & Katayama, Y. (2021). Ion solvation and water structure in an aqueous sodium chloride solution in the gigapascal pressure range. *Journal of Physical Chemistry Letters*, *12*(1), 250–256. https://doi.org/10.1021/acs.jpclett.0c03147

Yardley, B. W. D., & Bodnar, R. J. (2014). Fluids in the continental crust. *Geochemical perspectives* (Vol. 3). European Association of Geochemistry. Retrieved from https://pubs.geoscienceworld.org/perspectives/article-abstract/3/1/1/217791/fluids-in-the-continental-crust?redirectedFrom=fulltext

Yardley, B. W. D., & Valley, J. W. (1997). The petrologic case for a dry lower crust. *Journal of Geophysical Research*, *102*(6), 12173–12185. https://doi.org/10.1029/97JB00508

Yoshino, T., Gruber, B., & Reinier, C. (2018). Effects of pressure and water on electrical conductivity of carbonate melt with implications for conductivity anomaly in continental mantle lithosphere. *Physics of the Earth and Planetary Interiors*, *281*, 8–16. https://doi.org/10.1016/j.pepi.2018.05.003

Yoshino, T., & Noritake, F. (2011). Unstable graphite films on grain boundaries in crustal rocks. *Earth and Planetary Science Letters*, *306*(3–4), 186–192. https://doi.org/10.1016/j.epsl.2011.04.003

Zedgenizov, D. A., Rege, S., Griffin, W. L., Kagi, H., & Shatsky, V. S. (2007). Composition of trapped fluids in cuboid fibrous diamonds from the Udachnaya kimberlite: LAM-ICPMS analysis. *Chemical Geology*, *240*(1–2), 151–162. https://doi.org/10.1016/j.chemgeo.2007.02.003

Zhang, B., & Yoshino, T. (2017). Effect of graphite on the electrical conductivity of the lithospheric mantle. *Geochemistry, Geophysics, Geosystems*, *18*(1), 23–40. https://doi.org/10.1002/2016GC006530

Zhang, R. Y., Liou, J. G., Iizuka, Y., & Yang, J. S. (2009). First record of K-cymrite in North Qaidam UHP eclogite, Western China. *American Mineralogist*, *94*(2–3), 222–228. https://doi.org/10.2138/am.2009.2983